

RSC Advances



This is an *Accepted Manuscript*, which has been through the Royal Society of Chemistry peer review process and has been accepted for publication.

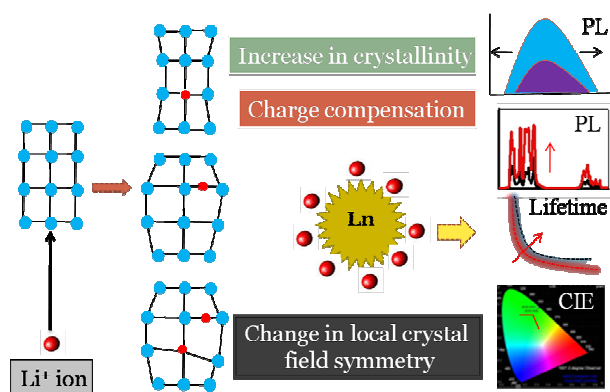
Accepted Manuscripts are published online shortly after acceptance, before technical editing, formatting and proof reading. Using this free service, authors can make their results available to the community, in citable form, before we publish the edited article. This *Accepted Manuscript* will be replaced by the edited, formatted and paginated article as soon as this is available.

You can find more information about *Accepted Manuscripts* in the [Information for Authors](#).

Please note that technical editing may introduce minor changes to the text and/or graphics, which may alter content. The journal's standard [Terms & Conditions](#) and the [Ethical guidelines](#) still apply. In no event shall the Royal Society of Chemistry be held responsible for any errors or omissions in this *Accepted Manuscript* or any consequences arising from the use of any information it contains.

Graphical Abstract

The effect of alkali ions on the modification of various host matrices and its effects on the luminescence properties of lanthanide ions have been demonstrated in this comprehensive review.



Dr. A. K. Singh

Akhilesh Kumar Singh is a Postdoctoral Fellow in the Instituto de Ciencias Físicas, Universidad Nacional Autónoma de México, Cuernavaca, México. He holds M. Sc. in Physics (2004) from V.B.S. Purvanchal University, Jaunpur, India and M. Tech. (2007) and Ph.D. (2012) in Materials Science and Technology from Indian Institute of Technology (Banaras Hindu University) Varanasi, India. His research interests include synthesis, characterization and application of lanthanide-based novel luminescent materials, nanostructure and quantum dots. He has published 18 peer-reviewed International journal papers and is a co-investigator of an Indian Patent.

Dr. S. K. Singh

Sunil K Singh, born in 1982, received doctoral degree in Physics in 2011 from the Banaras Hindu University, India. Currently, he is DST-INSPIRE faculty at Indian Institute of Technology (Banaras Hindu University), Varansi, India. His research interest includes Physics of multimodal luminescence (upconversion, downconversion/quantum-cutting, downshifting) in lanthanide and/or semiconductor quantum dot doped nanostructures. In terms of applications, the focus is on bio-imaging, to increase the conversion efficiency of photovoltaic cells, sensors, and for security purposes, *etc.* He has authored/co-authored a book chapter and more than 30 articles in peer-reviewed journals, and his current h-index is 9 (April 2014).

Professor S. B. Rai

S. B. Rai is professor in the Department of Physics, Banaras Hindu University, Varanasi, India since 1994. He did Ph.D. (Physics) in 1974 from Banaras Hindu University and visited Germany as Alexander von Humboldt fellow during 1982-84 and several time later on. His current interest of research includes multifunctional materials doped with rare-earth ions e.g. glasses, ceramics, phosphors, quantum dots, polymers, hybrid nanostructures, etc and their applications in various emerging fields. He has edited three books and several book chapters, and authored/co-authored around 300 articles in peer-reviewed national and international journals.

**Role of Li⁺ ion in the luminescence enhancement of lanthanide ions:
Favorable modifications in host matrices**

A. K. Singh^{1,2*}, S. K. Singh³, S. B. Rai¹

¹Department of Physics, Banaras Hindu University, Varanasi-221005, India

²Instituto de Ciencias Físicas, Universidad Nacional Autónoma de México, Cuernavaca, Morelos
C.P. 62210, México

³Department of Physics, Indian Institute of Technology (Banaras Hindu University) Varanasi-
221005, India

Abstract

Lanthanide based materials are being preferred over other luminescent materials for various applications. Current focus in this area is to exploit unique luminescence features of lanthanide-based materials for multidisciplinary research and novel applications. Furthermore, efforts are going on to enhance the luminescence of lanthanide ions for better performance. In broader sense, there are two ways to enhance the luminescence of lanthanide ions. The first is to use a suitable sensitizer, which can absorb excitation energy, efficiently, and can transfer it to the lanthanide ions. This method is known from long time and is well documented in literature. The second way is to modify host matrices in such a way that it favors radiative transitions. It is widely reported in literature that, the presence of alkali ions, particularly Li⁺ ion, in a matrix enhances the luminescence of lanthanide ions, significantly. But there is no any comprehensive note available in literature which summarizes that, how alkali ions help in the luminescence enhancement of lanthanide ions in various host matrices. The prime objective of this review is to highlight various contributing factors which help in the luminescence enhancement of lanthanide ions in the presence of alkali ions.

Keywords: Alkali, lanthanide, luminescence, crystal field symmetry, charge compensation, rare earth

*Corresponding author: Email: akhilesh_singh343@yahoo.com

Formatted: Font color: Black

Formatted: Font color: Black

Formatted: Font color: Black

1. Introduction

Lanthanide ions exhibit fascinating optical properties, including the ability to convert near infrared photons to ultraviolet/visible photons (through upconversion process) and vice-versa (quantum-cutting process).¹⁻⁵ Due to their unique optical features many of the advance and emerging applications such as lighting devices (light emitting diodes, economical luminescent lamps), optical fibres, display devices, lasers and many biological investigations are heavily depend on them.¹⁻⁵ Fundamentally, lanthanide ions have essentially three types of optical transitions: intra-configurational $4f-4f$ transition, inter-configurational $5d-4f$ transition and the charge transfer transition (ligand to metal or metal to ligand).⁵⁻⁶ Ce^{3+} and Eu^{2+} are widely used activator ions for phosphor applications.⁷⁻¹⁹ Their characteristic transition is $4f-5d$, which is an allowed transition and have lifetime of the order of nanosecond. Since, the $5d$ orbital are strongly affected by the crystal field and polarizability of the host crystal these transitions ($4f-5d$ transitions) can be easily tuned into visible regions by changing crystal composition and structure.⁷⁻¹⁹ In contrast, $4f-4f$ transition in lanthanide (III) ions (viz. Pr^{3+} , Nd^{3+} , Ho^{3+} , Er^{3+} , Sm^{3+} , Eu^{3+} , Tb^{3+} , Dy^{3+} , Tm^{3+} and Yb^{3+}), which is an forbidden transition, gives sharp and intense spectral lines (from UV to infrared region) with lifetime of the order of microsecond.²⁰⁻³⁰ Further, as the $4f$ orbital remain shielded by $5s$ and $5p$ orbitals, $4f-4f$ transitions are very less influenced by external environments (crystal field of host matrices).²⁰⁻³⁰

In recent years, research in the lanthanide-based luminescence materials are focused to exploit the unique features of lanthanide in various other novel applications viz. for multimodal emission (downconversion (DC)/quantum-cutting (QC), down-shifting (DS) as well as upconversion (UC) processes) based imaging, in increasing the efficiency of solar cell (by using an additional DC/UC layer in solar cell to minimize the thermal and sub-bandgap losses), as contrast agent in magnetic resonance imaging, various biological applications, etc.³¹⁻³⁵ The

pragmatic implication of luminescence materials for these applications demand efficient material in many ways, including an increase in the emission intensity. Therefore, continuous active research efforts in this field are desired to enhance the luminescence intensity of the lanthanide ions.

There are two fundamental ways to enhance the luminescence intensity of the lanthanide ions in a given host. The first is to use a suitable sensitizer, which can absorb UV and/or NIR radiations effectively and can transfer the energy to the central lanthanide ions.^{1-3, 36-42} In literature, different sensitization strategies are reported for increasing the luminescence of lanthanide ions viz. by forming lanthanide ion complexes with organic ligand, which can strongly absorb UV radiation and transfer efficiently to the central lanthanide ion; by excited state energy transfer from the charge transfer band to the lanthanide ion; by using co-dopant and thereby energy transfer among lanthanide themselves, *etc.*^{24, 38, 41} The second way to enhance the luminescence of lanthanide ions is to modify the host matrices in such a way that it favors transitions of lanthanide ions. Due to smaller ionic radius alkali ions, particularly Li^+ ion is very frequently used now days for this purpose.^{7-19, 56-142} Li^+ ion can easily get accommodated in host matrices, and tailors the local crystal field around the lanthanide ions.

Recently, our group has also worked in this line and shown that, the use of Li^+ ion enhances the photoluminescence (PL) of lanthanide ions in YPO_4 and Y_2O_3 host.^{74, 81, 84} In literature several models have been proposed by different groups to explain the luminescence enhancement in the lanthanide ions in different host matrices.⁵⁶⁻¹⁴² However, to the best of our knowledge, there is no any review article which summarizes a comprehensive view about, how the alkali ion modifies a host matrix which results enhanced luminescence. The prime objective of this review is to fill this gap and highlight various contributing factors which work in the

luminescence enhancement, in particular. Along with this, since different types of host matrices have been reviewed individually through the entire course work, so the present article could also be very useful in studying/visualizing the role of matrix on luminescence intensity of lanthanide ions, in general. This review is written in such a way that, it could be useful for a broad audience of chemists/biochemists and materials scientists as well.

2. Basics of lanthanide luminescence

The term lanthanide originated from a Greek word *lanthaneien* meaning “lying hidden”. Lanthanide is a family of 15 chemically similar elements, from lanthanum to lutetium (atomic number 57 to 71), which possess electronic configuration $[\text{Xe}] 4f^n 5d^{0,1} 6s^2$ (where ‘n’ varies from 0-14).⁵⁻⁶ Scandium (21) and yttrium (39) (d-block elements) are found in nature always with lanthanide; therefore, lanthanide and these two elements altogether known as rare-earth elements. Lanthanide exist usually in +3 oxidation state (Ln^{3+}) which is their most stable oxidation state (though Eu^{2+} , Sm^{2+} and Cr^{4+} also exist) and most of the optical properties of lanthanide are explored in this oxidation state. As the lanthanide ion feature an electron configuration of $4f^n$, which offers large number of possible arrangements, there are rather large numbers of electronic levels.

The promotion of $4f$ electron into the $5d$ sub-shell in lanthanide ions are allowed by the parity rule. These transitions are quite energetic and observed only in Ce^{3+} , Pr^{3+} and Tb^{3+} ions. Since the $5d$ orbitals are external and interact directly with the ligand orbitals their energy largely depends on metal environment.⁷⁻¹⁹ In Ce^{3+} ions, luminescence observed from $^2\text{D}_{3/2}$ levels to $^2\text{F}_{5/2}$, $^2\text{F}_{7/2}$, whereas $^2\text{D}_{5/2}$ lies at high energy and luminescence from this level is not generally observed. The luminescence in Ce^{3+} can be tuned from about 290 to 450 nm, depending on the matrix into which the metal ion is inserted. The charge transfer transition in lanthanide ions is also allowed

by Laporte's selection rule. The other and most studied transition in lanthanide is $4f-4f$ transitions. According to Laporte's rule electric dipole transition with the same parity are not allowed. By virtue of that, $4f-4f$ transition in lanthanide is forbidden.⁵⁻⁶ However, when these ions are doped in a suitable host matrix, due to influence of ligand-field, non-centrosymmetric interactions, a mixing of the wavefunctions of the states of opposite parity with $4f$ -wavefunctions takes place. This relaxes somewhat parity selection rule and $4f-4f$ transitions becomes partially allowed.⁵⁻⁶ Furthermore, the crystal field destroy the degeneracy of its energy levels. In fact, ligand/crystal generates a ligand/crystal electrostatic field which, in turn, interacts with the $4f$ electrons of lanthanide ions generating a ligand-field/crystal-field (or Stark) splitting of the spectroscopic levels.⁵⁻⁶ The $4f$ orbital of the lanthanide ions remain shielded by $5s$ and $5p$ orbital, and therefore promotion of an electron into a $4f$ suborbital of higher energy does not change the binding pattern, significantly. Thus, the inter-nuclear distance remains almost unchanged in the excited state, which produces narrow emission lines. The long lifetime is because of the fact that, the $4f-4f$ transitions in the lanthanide ions are parity forbidden.⁵⁻⁶ Table 1 summarizes the energy of principal $4f-4f$ transitions of lanthanide ions coming through DS, QC and UC processes.

The $4f-4f$ transition in lanthanide ions facilitates UC, DC/QC as well as DS processes, which may allow for facile photon management.⁴³⁻⁵¹ In DC/QC process, an incident higher-energy photon splits into two (or more) lower energy photons with conversion efficiency more than 100%.⁴⁶⁻⁴⁹ DS is similar to QC but it is a single photon process that involves the transformation of one absorbed high-energy photon into one low-energy photon and so its conversion efficiency does not exceed 100%.⁵⁰⁻⁵¹ While, on the other hand, UC is a nonlinear process which involves two or more low energy photons (usually NIR) to emit a single photon of

higher energy (usually visible or ultraviolet).⁴³⁻⁴⁵ To generate practically useful UC emission, the energy difference between each excited level and its lower-lying intermediate level (ground level) should be close enough to facilitate photon absorption and energy transfer steps involved in UC processes. Er^{3+} , Tm^{3+} , and Ho^{3+} typically feature such ladder-like arranged energy levels and are thus frequently used activators.

Selection of appropriate host matrix for the preparation of lanthanide-based luminescence material is an essential requirement. As the luminescence of lanthanide ions is very sensitive to the local crystal field environment, host matrix should have close lattice matches to the dopant ions.⁵²⁻⁵⁴ Failing to this can create large distortion in the matrix which strongly influences the luminescence of lanthanide ions. Particularly, the $5d-4f$ transitions of the lanthanide ions are strongly influenced (both position and intensity) by the crystal field of the matrix.⁷⁻¹⁹ Since the lanthanide (III) ions exhibit similar ionic size and chemical properties their inorganic compounds are ideal host for lanthanide ions doping. In addition, alkaline earth ions (Sr^{2+} , Ca^{2+} , and Ba^{2+}) and some transition metal ions (Zr^{4+} and Ti^{4+}) also exhibit close ionic size to lanthanide ions and are frequently used as host materials for lanthanide ions doping. Further, the ideal host matrix should also have low lattice phonon energies, to minimize non-radiative loss and maximize the radiative emission. The dopant concentration, which determines the average distance between neighboring dopant ions, has a strong influence on the optical properties of the lanthanide-based luminescence materials.⁵²⁻⁵⁴ In certain host matrices, luminescence of lanthanide ions increases appreciably with increasing crystallinity. This is because of the fact that, as the crystallinity increases the particle size also increases, which reduces surface quenching centers (surface to volume ratio decreases). The increased particle size is not required in many technological applications, specially triggered due to the advancement in

nanotechnology,; therefore, researchers usually like to use a passive layer, by forming core-shell structure, to reduce the surface quenching centers.⁵⁴ The co-doping of alkali ions in the matrix strongly affects the crystal structure, crystallinity, grain-size, surface morphology, quenching centers (OH^- , NO_3^- , *etc.*) and create distortion in the matrix.⁵⁶⁻¹⁴² Therefore, it would be interesting to study the effect of alkali ions, particularly Li^+ ion, on the luminescence properties of lanthanide ions doped in various matrices and try to find out some meaningful information to understand the mechanism behind, and also to explore the future possibilities. The following sections aim to investigate these aspects in detailed.

3. Effect of Li^+ ion on the luminescence of Ce^{3+} and Eu^{2+} ($5d-4f$ transition) ions

As discussed in the preceding sections, the origin of luminescence from Ce^{3+} and Eu^{2+} ions is different from the characteristic luminescence of lanthanide (III) ions involving $4f-4f$ transitions. The luminescence in Ce^{3+} and Eu^{2+} ions is due to $4f^{n-1}5d^1$ to $4f^n$ (ground state) transition (where, $n=7$ for Eu^{2+} and 1 for Ce^{3+}).⁷⁻¹⁹ These transitions are allowed and have lifetime of the order of nanosecond. They exhibit broad-band luminescence spectrum, with their maxima lying in yellow region, and are very useful for lighting applications (LEDs, automobile lamps, and backlighting, *etc.*). As the $5d$ orbitals are external, the position of these levels and thereby the excitation and emission bands strongly depend on the local environment of the ions (crystal fields of the host matrices). Dorenbos⁵⁵ has made a clear correlation between the coordination polyhedron (in which Eu^{2+} or Ce^{3+} lies) and the crystal field splitting. They have shown that the crystal field splitting tends to be the largest for octahedral coordination followed by cubal, dodecahedral, and it is the smallest for tricapped trigonal prism and cuboctahedron coordination. Thus, through appropriate host selection (with different crystal field splitting of the $5d$ band), the luminescence of Eu^{2+} and Ce^{3+} can be tuned according to the requirement. Part *et al.* have shown that Eu^{2+}

doped Sr_2SiO_4 and Sr_3SiO_5 are stronger yellow emitting phosphor than the conventional light-conversion phosphor $\text{YAG}:\text{Ce}^{3+}$.⁸ Co-doping of Li^+ ion with $\text{Eu}^{2+}/\text{Ce}^{3+}$ not only improves the luminescence efficiency but brings out changes even in excitation and emission spectral range, so both these activators ions have been effectively studied in presence of Li^+ ions. Table 2 gives a brief detail of different host and dopant ions which have been studied to visualize the effect of Li^+ co-doping.

Grandhe *et al.*¹² investigated the effect of Li^+ ion on the emission characteristics of Eu^{2+} emission in phosphate matrix ($\text{Na}_{1-y}\text{Li}_y\text{Ca}_{1-x}\text{PO}_4:\text{xEu}^{2+}$) synthesized by conventional solid state reaction method. The excitation spectra of $\text{NaCaPO}_4:\text{Eu}^{2+}$ phosphors revealed a broad excitation band ranging from 250 to 450 nm with maximum intensity at 373 nm. On 373 nm excitation, the phosphor exhibits intense bluish-green emission band centered at 505 nm. Fig. 1 (b) shows that $\text{Na}_{1-y}\text{Li}_y\text{Ca}_{0.99}\text{PO}_4:0.01\text{Eu}^{2+}$ phosphor containing 4 mol% of Li^+ ions ($y=0.04$) exhibits maximum luminescence intensity. It is suggested that the difference in the ionic radii probably give rise to diversity in the crystal lattice around the luminescence center. This may inturn influences the spin-orbit coupling and the crystal field around the Eu^{2+} ions. Liu *et al.*⁸ have synthesized $\text{Li}_2\text{CaSiO}_4:\text{Eu}^{2+}$ phosphor by conventional solid state reaction method and found that Li^+ ion changes the excitation and emission characteristics of Eu^{2+} effectively in silicate matrix also. It was again concluded due to the change in host lattice/crystal field due to the involvement of Li^+ ions in the crystal structure. They proposed that the Eu^{2+} ions goes to distorted dodecahedral Ca sites, which causes strong crystal field splitting leading to a broad excitation band extending from UV to visible region. Also, the high concentration of Li^+ ions in the structure constrained the distortion of the emission center (Li^+ ions, which are behind the oxygen ions surrounding the

emission centers, will restrict the expansion of the emission centers), which results smaller Stokes shift.

Similar study for Ce^{3+} doped in silicate matrix has also been presented by Zhu *et al.*¹⁶ Authors have prepared $\text{Sr}_3\text{SiO}_5: \text{Ce}^{3+}, \text{Li}^+$ phosphor, by solid state reaction method, and showed that under the near-UV excitation of 415 nm, the phosphor emits a bright greenish-yellow color centered at 532 nm (originates from $5d$ to $4f$ ($^2F_{7/2}$ and $^2F_{5/2}$) transition of Ce^{3+}). On substitution of Sr^{2+} ions with Mg^{2+} (smaller ionic radius than Sr^{2+}) and Ba^{2+} (larger ionic radius than Sr^{2+}) ions the peak position of PL spectrum shifts towards higher and lower energy, respectively. This is because of the fact that, as Mg^{2+} ions substitutes Sr^{2+} ions the degree of covalence in the Ce–O bonds is decreased, and consequently less negative charges transfer to Ce^{3+} ions and thus increase the difference between the $4f$ and the $5d$ levels (causes blue-shift in emission band). In contrast, the substitution of Sr^{2+} with larger Ba^{2+} increases the degree of covalence in the Ce–O bonds, which causes redshift in the emission band. Thus, the emission color of $\text{Sr}_3\text{SiO}_5: \text{Ce}^{3+}, \text{Li}^+$ can be tuned by partially replacement of Sr^{2+} with Mg^{2+} or Ba^{2+} , which make it apply to a variety of LEDs (from 410–450 nm chips). In another similar article by Shen *et al.*¹⁴, role of Li^+ have been proposed in the same host in more detail, which explores that the Li^+ codoping compensates the charge difference between the Ce^{3+} and Sr^{2+} ions and thus helps to incorporate the Ce^{3+} into Sr^{2+} sites. The phosphor ($\text{Sr}_3\text{SiO}_5: \text{Ce}^{3+}, \text{Li}^+$) shows high luminous efficiency under near-UV/blue light excitation, and the obtained emission is comparatively broader than that of Eu^{2+} -activated yellow phosphor. To improve the color rendering properties of $\text{Sr}_3\text{SiO}_5: \text{Ce}^{3+}, \text{Li}^+$ phosphor, Jang *et al.*¹⁸ have used additional Pr^{3+} (to enhance the red-emitting component) ions along with Ce^{3+} ions. Under blue light excitation energy transfer from Ce^{3+} to Pr^{3+} ions take place which gives a shoulder at 619 nm (of Pr^{3+} ions) in the PL spectrum of $\text{Sr}_3\text{SiO}_5: \text{Ce}^{3+}, \text{Pr}^{3+}, \text{Li}^+$. The

energy transfer has been proved by steady-state and time domain luminescence measurements. Further, by making use of monodisperse CdSe QDs and the phosphor onto a blue LED chip, they produced white LEDs with excellent color rendering property (see Fig.1 (d) and (e)).

Wang *et al.*¹⁷ have prepared CaSiN₂ powders at 1550 °C in a N₂/H₂ (6%) atmosphere by solid-state reaction method using Ca₃N₂ and Si₃N₄ as the starting materials. The luminescence measurements on Ce³⁺/Li⁺ co-doped CaSiN_{2-2δ/3}O_δ shows a broad yellow band peaking at 530 nm. The maximum PL intensity was attained for the sample with the Ce³⁺ composition x = 0.01, above this concentration quenching occurs. The oxygen content in the sample was analyzed and is found to be δ ≈ 0.2. Further, the chromaticity coordinates (0.362, 0.571) also demonstrate that CaSiN_{2-2δ/3}O_δ: Ce³⁺/Li⁺ is a good yellow phosphor (see Fig 1 (a)). Hao *et al.*¹⁰ studied PL properties of CaO: Ce³⁺, Li⁺ phosphor. It is found that, on 474 nm excitation, Li⁺ ions co-doped phosphor shows 1.88 times enhancement in PL intensity (see Fig 1(c)). The XRD results shows the presence of small amount of CeO₂, a raw material, in CaO:Ce³⁺ phosphor which suggests low solubility of Ce³⁺ in CaO. On Li⁺ ion co-doping the intensity of this peak decreases, indicating that more CeO₂ is converted to Ce³⁺ ions for effective doping into CaO host lattice. This results increased absorption of the excitation photons in CaO: Ce³⁺, Li⁺ causing PL enhancement. This might be because of the charge compensation due to presence of Li⁺ ions and effect of Li⁺ as a flux to increase diffusivity of the raw materials which causes more Ce³⁺ ions to go into CaO lattice. Jia *et al.*¹⁵ have prepared Lu₂SiO₅:Ce³⁺, Li⁺ phosphor by Pechini sol-gel chemistry. They optimized the concentration of Ce³⁺ and Li⁺ ions and it was found to be 0.006 wt. % and 0.02 wt. %, respectively. The PL intensity of 0.006 wt. Ce³⁺, 0.02 wt.% Li⁺ co-doped phosphor sample was 2.2 times higher than the 0.006 wt. Ce³⁺ doped phosphor. It is suggested that the Ce³⁺ ions occupy two different crystallographic sites (with coordination number 6 or 7) in the monoclinic

lattice (space group $C2/c$) of Lu_2SiO_5 .¹⁴³ This causes two luminescent centers Ce1 and Ce2 in this host. The peaks at 3.16 and 2.95 eV originate from the emission of the Ce1 center, while another peak at 2.74 eV corresponds to the Ce2 center. With the increase of (Li^+ ion) co-doping concentration, initially the intensity of Ce1 emission increases and then decreases, while the Ce2 emission intensity always decreases. This suggests the energy transfer from Ce2 to Ce1 centers which was demonstrated by time-domain measurements. Thus the enhanced luminescence of $\text{Lu}_2\text{SiO}_5:\text{Ce}^{3+}$ phosphors by Li^+ ion co-doping is mainly regarded as the result of the production of the local distortion in host lattice, which alters the crystal field around activator and results in the energy transfer from Ce2 to Ce1 centers.¹⁵

The effect of Li^+ ions have been investigated for persistent/afterglow emission also. Kojima et al.⁹ have studied afterglow luminescence properties of green emitting Ce^{3+} and Pr^{3+} co-doped CaS phosphor. The afterglow time of $\text{CaS}:\text{Ce}^{3+}$, Pr^{3+} was relatively short (about 10 min). When Li^+ is introduced in the matrix, the afterglow intensity and afterglow time of $\text{CaS}:\text{Ce}^{3+}$, Pr^{3+} both increases, by three and four times, respectively. It is shown that the Li^+ ions go to interstitial spaces in the crystal lattice and increases the lattice constant. When a Li^+ ion is incorporated into the crystal lattice of CaS, new cation vacancy is formed for the charge compensation in the Ca^{2+} site, which increases the lattice strain. This cation vacancy working as an electron trap can capture some of the excited electrons and thereby increases the charging process. Chen *et al.*¹¹ have prepared $\text{SrAl}_2\text{O}_4:\text{Eu}^{2+},\text{Ce}^{3+},\text{Li}^+$, another persistent luminescence material, by solid-state reaction method using H_3BO_3 as flux. Li^+ ions compensate the charger defects caused by the non-equivalent substitution of Sr^{2+} with Ce^{3+} . Thus, the luminescence intensity of $\text{SrAl}_2\text{O}_4:\text{Eu}^{2+}$ is significantly enhanced when Ce^{3+} and Li^+ both are present in the sample.

4. Effect of Li⁺ ion on the luminescence of lanthanide (III) ions coming through 4f-4f transitions

4.1 Effect of Li⁺ ion on the luminescence of lanthanide ions in yttrium oxide (Y₂O₃) and gadolinium oxide (Gd₂O₃) host matrices

Y₂O₃ and Gd₂O₃ are well explored host matrices for luminescence studies owing to their higher chemical and mechanical durability, higher thermal stability, excellent optical properties and relatively low phonon cutoff energy (400-500 cm⁻¹) in comparison to the other host matrices.¹⁴⁴⁻¹⁵⁰ Another advantage of using Y₂O₃ and Gd₂O₃ host matrix is that, one can easily prepare phase pure samples by conventional solid state reaction (at lower temperatures) method and also by many other routes (such as solution combustion technique, sol-gel technique, hydrothermal technique, *etc.*).¹⁴⁴⁻¹⁵⁰ Furthermore, particle size, shape and surface morphology can be tuned/controlled easily by controlling different synthesis parameters. Moreover to this, ionic radius of Y³⁺ and Gd³⁺ is almost similar to the other activator lanthanide ions; thus they can easily be accommodated in the matrix.¹⁴⁴⁻¹⁵⁰ Gd₂O₃ exhibits paramagnetic behavior therefore the phosphor prepared using this host is important for bio-imaging, MRI contrast reagent, *etc.*¹⁴⁸⁻¹⁵⁰

Recently, several research groups, including our own, have used Li⁺ ion to further enhance the luminescence of lanthanide ions doped in this matrix.⁵⁶⁻⁷⁴ Table 3 summarizes the concentrations of different activator (lanthanide) ions and Li⁺ ion for getting the optimum luminescence. The table also describes the mode of luminescence measurement (e.g. DS, UC), quantitative information about luminescence enhancement and the explanation given by different research groups for luminescence enhancement. It is evident from the table 3 that, different research groups have proposed different mechanism for luminescence enhancement of lanthanide

activator ions in presence of Li^+ ion. A detail description of the work done so far and their salient features are summarized ahead including the detail description of the representative works in the area concerned.

Dhananjaya *et al.*⁵⁸ studied the effect of Li^+ ion on the PL of Eu^{3+} in Gd_2O_3 host. They proposed that when the concentration of Li^+ ion in the Gd_2O_3 host is low (<4 mol %) substitution of Gd^{3+} ion with Li^+ ion induces oxygen vacancies. This causes crystal field distortion around activator ion (Eu^{3+}) which results increased PL. The oxygen vacancies also act as a sensitizer for activator lanthanide ions, by the involvement of an effective energy transfer from the strong charge transfer states (come into picture due to vacancy itself) to lanthanide ions. Further, they explore that, as the Li^+ concentration increases, along with substitutional Li^+ site, interstitial site of Li^+ ion are also present that causes Gd^{3+} ion vacancies. This as a result produces more defects around the activator lanthanide ions. In this case the Stark level in the emission spectrum shows larger splitting. In a similar study, Shin *et al.*⁵⁷ have monitored cathodoluminescence (CL) of Eu^{3+} ion in Gd_2O_3 and Y_2O_3 both the host matrices in the presence of Li^+ ion, and they also proposed the charge compensation mechanism for CL enhancement of Eu^{3+} ions in both the host, while for the case of Gd_2O_3 host the group additionally put forward other mechanisms also described in the subsequent paragraph.

Alongwith charge compensation mechanisms, several other mechanisms for the luminescence enhancement have also been reported. The cubic structure of Y_2O_3 and Gd_2O_3 offers two different crystallographic sites to activator lanthanide ions, one with C_2 (without center of inversion) and the other with S_6 (with center of inversion (C_{3i})) symmetry.⁵⁷ The transitions in lanthanide ions are affected effectively, as far as the intensity and splitting is concerned, by the symmetry of the crystal field of host. For example, when Eu^{3+} ion occupies S_6

symmetry, the magnetic-dipole transition ${}^5D_0 \rightarrow {}^7F_1$ is the dominant one. In case of Eu^{3+} doped material the occupancy ratio of two different sites (ORS) i.e. local symmetry around Eu^{3+} ion can be easily obtained by taking the intensity ratio of ${}^5D_0 \rightarrow {}^7F_2$ (~611 nm) to ${}^5D_0 \rightarrow {}^7F_1$ (~590 nm) transitions.⁵⁷ Ionic radii of Y^{3+} , Gd^{3+} and Li^+ ion are 0.89, 0.94 and 0.76 Å, respectively.^{57, 58} Thus, Li^+ ion substitution deforms Gd_2O_3 lattice more as compared to Y_2O_3 lattice, and the statistical distribution of lanthanide (Eu^{3+}) and Li^+ ion at the C_2 and S_6 sites in Gd_2O_3 lattice becomes more intricate. Shin *et al.*⁵⁷ have also reported that, change in ORS after Li^+ ion incorporation is larger in Eu^{3+} doped Gd_2O_3 than Y_2O_3 matrix. Based on this information, Shin *et al.* proposed that the mechanism of luminescence enhancement in Li^+ ion doped Gd_2O_3 might be different than in Y_2O_3 host. X-ray diffraction (XRD) patterns (shown in Fig.2) recorded by Shin *et al.*⁵⁷ reveals that $\text{Y}_{1.95-x}\text{Li}_x\text{O}_3:\text{Eu}_{0.05}$ phosphor samples have cubic structure even for higher doping concentration of Li^+ ion. In contrast, $\text{Gd}_{1.95-x}\text{Li}_x\text{O}_3:\text{Eu}_{0.05}$ phosphor samples show monoclinic to cubic transformation as the doping concentration of Li^+ increased. This gradual change from monoclinic to cubic lattice is also confirmed by Dhananjaya *et al.*⁵⁸ This change in monoclinic to cubic lattice in Gd_2O_3 host is also one of the reasons for increased luminescence.^{57, 58}

Fan *et al.*⁶² have reported the effect of Li^+ ion in enhancing the PL of Nd^{3+} ion doped in Y_2O_3 samples. They proposed that, among two different crystallographic sites (C_2 and C_{3i}) symmetry, the ratio of C_2 to C_{3i} sites is 3:1 of cubic Y_2O_3 , electric-dipole transitions of lanthanide ions are forbidden for C_{3i} sites. Thus, when Li^+ ions occupy the C_{3i} sites, it destroys the inversion symmetry and the forbidden electric-dipole transitions of lanthanide ions (Nd^{3+}) become partially allowed. Further, when Li^+ ions are occupying the C_2 sites with higher population in the lattice, the reduced symmetry of these sites again results in the enhancement of

PL of lanthanide ions (Nd^{3+}). Thus, in both the cases enhanced PL is observed. When the Li^+ ion concentration is too high it might cause a large local distortion around optically active centers (lanthanide ions) which can lead to the PL quenching.

In similar context, several studies have been reported for the enhancement of UC emission also. Study by Sun *et al.*⁶⁰ reports the UC phenomena in silica coated $\text{Tm}^{3+}/\text{Yb}^{3+}/\text{Li}^+$ ions doped Gd_2O_3 matrix, and found ~10 times enhancement of UC emission in the sample doped with 6 mol % of Li^+ . They have suggested that the enhancement in PL is due to change in the local asymmetry around Tm^{3+} ions. On further increasing the Li^+ ions concentration (up to 10 mol %) the UC emission decreases substantially. They have reported that at higher Li^+ ion concentrations local crystal field around Tm^{3+} ions yet again became symmetric, which is unfavorable for UC emission. Chen *et al.*⁶⁴ ($\text{Yb}^{3+}/\text{Er}^{3+}$), Bai *et al.*⁶⁵ ($\text{Yb}^{3+}/\text{Er}^{3+}$), Li *et al.*⁷¹ ($\text{Yb}^{3+}/\text{Er}^{3+}$), Fan *et al.*⁷² (Yb^{3+}) and Mishra *et al.*⁷⁴ ($\text{Yb}^{3+}/\text{Er}^{3+}$) have also studied the effect Li^+ ion on the enhancement of UC/PL of lanthanide ions in Y_2O_3 and Gd_2O_3 host matrices and suggested the change in crystal symmetry around the lanthanide ions as one of the reasons for PL enhancement.

The other contributing factors in the PL enhancement of lanthanide ions in these hosts are change in morphology, crystallinity and grain size of materials.^{56, 59, 68, 69} Atomic force microscopy (AFM), which is used to study the surface morphology, results reported by Jeong *et al.*⁵⁶ shows that the Li^+ ion doping increases the grain size and roughness of the $\text{Gd}_2\text{O}_3:\text{Eu}^{3+}$ films. Larger grain size reduces density of the grain boundaries which in-turn might be responsible for reduced adsorption and/or scattered light generated inside the film which favors PL enhancement. Furthermore, increased crystallinity due to Li^+ ion doping in samples causes higher oscillating strength for optical transitions which also favors PL enhancement.⁵⁶ Yi *et al.*⁵⁹

(Gd₂O₃: Eu³⁺), Fan *et al.*⁶² (Y₂O₃: Nd³⁺), Yi *et al.*⁶⁸ (Y₂O₃: Eu³⁺) and Sun *et al.*⁶⁹ (Y₂O₃: Eu³⁺) have also proposed that increased grain size, roughness and crystallinity of materials, in presence of Li⁺ doping, is among one of the potential reasons for luminescence enhancement of lanthanide ions.

Time-domain studies have also been exploited to search for the possible reasons behind the enhancement of PL/UC emission. It has been observed that, change in lifetime of intermediate state/states participating in energy transfer process also plays a crucial role. Chen *et al.*⁶⁴ suggested that due to change in local crystal field of Y₂O₃ matrix around the lanthanide ions observed lifetime of intermediate states, ⁴I_{11/2} (Er³⁺) and ²F_{5/2} (Yb³⁺), can change. This can also modify the theoretical lifetimes of lanthanide ions by slightly changing their wavefunctions. They monitored decay profiles of ⁴I_{11/2} → ⁴I_{15/2} transition of Er³⁺ ion (at 1015 nm) in Y₂O₃ nanocrystals in the presence of 0–15 mol % Li⁺ ions (see Fig 3(d)).^{66, 67} Lifetime of the intermediate state ⁴I_{11/2} was found to be 0.8(2) ms and 2.7(3) ms for 0 and 3 mol % Li⁺ ions, respectively, and it is about 3.4(3) ms for higher Li⁺ ions concentrations (5–15 mol %). This suggest that local crystal field around Er³⁺ ions is gradually tailored for lower doping concentration of Li⁺ ions (0–5 mol%) and becomes nearly constant for higher Li⁺ ion concentrations. The enhancement in UC emission has the same trend as the lifetime increases. Fig 3 (a) and (b) shows UC emission spectra of Er³⁺ doped Y₂O₃ in absence and presence of Li⁺ ions. In an another work, Fan *et al.*⁷³ monitored the decay profiles of ⁴I_{13/2} → ⁴I_{15/2} transition (at 1530 nm) of Er³⁺ ions in Y₂O₃ matrix in the presence of 0–6 mol % of Li⁺ ion under the 976 nm excitation. They also observed an increase in the lifetime with increasing concentration of doped Li⁺ ion; the lifetime varies from 3.14 ms to 3.28 ms for 5 mol % Li⁺ ion. The study concludes and proposes that, the Li⁺ ion tailors the local crystal field around Er³⁺ ion, and therefore

modifies the theoretical lifetime by slightly changing the wavefunction, somewhat similar to the earlier reports.

Furthermore, some of the studies interestingly reports that the doping of Li^+ ion suppresses the PL quenching entities e.g. molecules with OH^- , NO_3^- , CO_x , etc. groups having high vibrational frequencies. During the phosphor synthesis by chemical routes (viz. combustion, sol-gel methods) incomplete combustion of organic fuel introduces luminescence quenching center which decreases the PL intensity. Sun *et al.*⁶⁰ ($\text{Gd}_2\text{O}_3:\text{Yb}^{3+}/\text{Yb}^{3+}$), Fan *et al.*⁶² ($\text{Y}_2\text{O}_3:\text{Nd}^{3+}$), Li *et al.*⁷¹ ($\text{Y}_2\text{O}_3:\text{Yb}^{3+}/\text{Yb}^{3+}$) and Mishra *et al.*⁷⁴ recorded FTIR (Fourier transform infrared) spectra of phosphor materials without and with Li^+ ion doping in various hosts and found that the broad absorption bands peaking at 1626 and 3454 cm^{-1} , owing to vibrational features of O–H groups are suppressed significantly in presence of Li^+ ion (see Fig 3(c)).⁷⁴ In addition, Mishra *et al.*⁷⁴ have also reported that the broad peak $\sim 1369 \text{ cm}^{-1}$, due to stretching vibration of NO in surface-adsorbed NO_3^- group, is also suppressed in presence of Li^+ . This might be due to the fact that the Li^+ ion neutralize the hydroxyl (and other) groups present in the phosphor. Thus, the addition of Li^+ ion reduces the non-radiative transition probability and hence enhances the PL efficiency.

Thus in summary, the Li^+ ion doping in Gd_2O_3 and Y_2O_3 host significantly affects both the structural and optical parameters such as charge compensation, change in crystal symmetry around activator ions, increased crystallinity, increased grain size, change in morphology (higher surface roughness), increase of lifetime of intermediate levels of activator ions, decrease in non-radiative channels (OH^- , NO_2^- concentrations), *etc.*, which altogether enhances the optical emission of lanthanide ions.

4.2 Effect of alkali ions on PL enhancement of lanthanide ions in ABO_4 type of compounds

Next to Y_2O_3 and Gd_2O_3 host matrices, another important class of compounds for PL studies belongs to ABO_4 (where, A is alkaline earth metal or trivalent lanthanide ion and B stands for hexavalent or pentavalent transition metal ion) family. There are some well known host of this family of compounds viz. $CaMoO_4$, YVO_4 , $GdVO_4$, $YNbO_4$, YPO_4 , $CaWO_4$, $MgWO_4$, $ZnWO_4$, etc. which have shown enormous interest in preceding years.^{83-85, 151-154} The characteristic feature of these compounds is existence of strong ligand (oxygen) to metal charge transfer band in UV region.¹⁵¹⁻¹⁵⁴ Under this charge transfer band excitation they exhibit broadband PL, mostly in blue region. Additional feature of this type of compounds is that they serve as sensitizer for the activator lanthanide ions by involving an energy transfer from charge transfer state to the resonant level of lanthanide ions, so they do not need co-dopant for sensitization process.²⁴ They are stable at high temperatures. Lanthanide doped YVO_4 is already explored for the fabrication of laser. Recently, different research groups across the world are studying the role of Li^+ on the PL enhancement of lanthanide ions in these hosts (alongwith other host matrices).⁷⁵⁻⁸⁸ Table 4 gives brief information about different host of this family, activator ions, maximum PL enhancement and the proposed mechanism to explain the PL enhancement. The following briefs about different mechanisms.

Compounds of this family usually have relatively large phonon cutoff range ($\sim 800\text{ cm}^{-1}$) than Y_2O_3 and Gd_2O_3 host matrices, and therefore, for getting efficient UC emission, sensitization becomes utmost essential. Chung *et al.*⁷⁶ have studied the role of Li^+ ion on UC emission of Er^{3+}/Yb^{3+} doped $CaMoO_4$ phosphor. They observed ~ 83 times enhancement in the green emission of Er^{3+} ion in the presence of 10 mol % of Li^+ ion (see Fig 4(b)). They have attributed it as being due to the favorable structural modification (change in local crystal field

symmetry) in the host lattice. The XRD patterns reveal that CaMoO_4 phosphor samples containing 2 mol % Er^{3+} , 8 mol% Yb^{3+} and 0-15 mol % Li^+ ion do not show any secondary phase. The diffraction peak (112) shifts gradually toward higher angle side up to 5 mol% Li^+ ion doping; however contrary to this, on further increasing Li^+ ion concentration it shifts toward smaller angle side (see Fig. 4(a)). The gradual peak shifts toward higher angle side below 5 mol% suggest that the Li^+ ion occupy the Ca^{2+} site in lattice. However, on further increasing the concentration of Li^+ ion it goes to interstitial site. This leads to the expansion of lattice. The occupation of Li^+ ion in the interstitial site distort the local crystal field around Er^{3+} ion, which plays an important role for the enhancement of UC emission.

Li *et al.*^{77,78} have also studied the effect of Li^+ ion in the same host, CaMoO_4 , but they have used Dy^{3+} and Tb^{3+} as the activator ions instead of Er^{3+} . To explain the PL enhancement for Dy^{3+} doped CaMoO_4 in the presence of Li^+ ion, they proposed that, as the ionic radius in the case of Dy^{3+} ion (0.091 nm) is similar to that of Ca^{2+} ion (0.099 nm) it can easily be accommodated into the Ca^{2+} site. However, the Li^+ ion which has considerably small radius (0.076 nm) will prefer to go into the interstitial spaces. The replacement of divalent calcium by trivalent dysprosium creates charge imbalance, and this imbalance is compensated by Li^+ ion co-doping, which enhanced the PL intensity, significantly. Further, in their another work, Li *et al.*⁷⁸ extends their observation for the effect of Li^+ , Na^+ and K^+ all the three for the PL enhancement of Tb^{3+} co-doped CaMoO_4 phosphors. A remarkable increase not only in PL, but for X-ray excited luminescence is also attained for all the three alkalis. The maximum PL was observed for 5 mol% Tb^{3+} and Na^+ doped phosphor. The study proposes that the enhanced PL is due to the creation of oxygen vacancies after the occupation of Ca^{2+} sites by alkali ions.

Phosphor samples ($\text{LaVO}_4:\text{Eu}^{3+}$) prepared by Park *et al.*⁸⁰ have both tetragonal and monoclinic phases. Between these two, the tetragonal phase of $\text{LaVO}_4:\text{Eu}^{3+}$ showed higher PL than monoclinic phase. Incorporation of Li^+ (0.25 wt. %) ion into the $\text{LaVO}_4:\text{Eu}^{3+}$ (0.07 mol %) phosphor increases the PL, remarkably. This is due to the fact that presence of Li^+ ion helps in monoclinic to tetragonal phase transformation which causes effective energy transfer from VO_4^{3-} to Eu^{3+} . Yang *et al.*^{86, 87} prepared Li-doped (0 to 3 mol %) $\text{YVO}_4:\text{Eu}^{3+}$ phosphors and observed that as the Li^+ ion content increases from 0 to 2 wt. %, the PL intensity got improved. The enhancement in PL intensity of 2 wt. % Li-doped $\text{YVO}_4:\text{Eu}^{3+}$ phosphor is ~ 1.43 in comparison to that of $\text{YVO}_4:\text{Eu}^{3+}$ ceramic (see Fig 4 (c)). They proposed that the enhanced PL is due to improvement in crystallinity as well as due to the enhanced surface roughness.

Parchur *et al.*^{81, 83-85} in our group have also studied the effect of Li^+ ion on PL properties of Dy^{3+} and Eu^{3+} doped YPO_4 phosphors. The Li^+ ion co-doping improves the crystallinity of the material and reduces agglomeration among the particles. On addition of Li^+ ion, the shift in (200) diffraction peak towards the lower 2θ value suggest that the Li^+ ion occupy interstitial site instead of $\text{Y}^{3+}/\text{Eu}^{3+}$ site. Furthermore, the Li^+ ion co-doping increases the crystallite size as well (crystallite size corresponding to $\text{Li}^+ = 0, 3, 5, 7$ and 10 at. % co-doped $\text{YPO}_4:\text{Eu}^{3+}$ are found to be 20, 23, 36, 42 and 60 nm, respectively). In the high resolution transmission electron microscopy (HRTEM) image (see Fig 4 (d)) of Li^+ and Eu^{3+} co-doped YPO_4 phosphor clear, damage free, visible lattice fringes indicates for a good crystallinity of the sample. This increased crystallinity and grain size causes significant enhancement in PL. Huang *et al.*⁸² have also proposed that the increased crystallinity is main cause for PL enhancement in Li^+ and Eu^{3+} co-doped YPO_4 phosphor (2.5 fold enhancement in 5% Li^+ and 5% Eu^{3+} co-doped YPO_4 than $\text{YPO}_4:5\%\text{Eu}^{3+}$).

Thus in summary, in Li^+ doped ABO_4 type of compounds, the main mechanism involved for the PL enhancement is change in local crystal field symmetry by modification in crystal lattice, mostly due to interstitial occupancy of Li^+ ion and development of vacancies. In addition to this, improvement in crystallinity, grain size, shape, *etc.* and energy transfer processes also have been accepted as potential mechanism as in other hosts too.

4.3. Effect of alkali ions on PL enhancement of lanthanide ions in calcium and strontium aluminates

Like Y_2O_3 and Gd_2O_3 , calcium and strontium aluminates also have low phonon frequency which makes them suitable for the lanthanide ion doping.¹⁵⁰⁻¹⁶⁰ Lanthanide doped phosphor material prepared using these hosts' exhibit good chemical stability and mechano-luminescence properties. Furthermore, aluminates are excellent host for the development of long persistence phosphors ($\text{CaAl}_2\text{O}_4:\text{Eu}^{2+}$, Dy^{3+} and $\text{CaAl}_2\text{O}_4:\text{Ce}^{3+}$) which makes them useful for display applications, delayed fluorescence, warning signals, emergency lighting and for other luminous products.¹⁵⁰⁻¹⁶⁰ Very recently, few publications have appeared on lanthanide doped aluminate hosts with Li^+ ion co-doping which shows an enhanced PL and the decay time.⁸⁹⁻⁹¹

Recently, Guanghuan *et al.*⁸⁹ studied the effect of alkali ions (Li^+ , Na^+ , K^+) on PL characteristics (both steady state and time-domain studies) of Eu^{3+} doped in CaAl_2O_4 phosphors. Optimum emission was obtained for 3 mol% of Eu^{3+} . Addition of alkali ions was found to enhance the PL intensity, significantly. The hypersensitive transition ${}^5\text{D}_0 \rightarrow {}^7\text{F}_2$ evolved as the most intense peak which was explained as Eu^{3+} ions occupy a low symmetry site. Since, the ionic radii of Eu^{3+} (0.095 nm) is close to Ca^{2+} (0.099 nm) than Al^{3+} (0.051 nm), therefore, it prefers to occupy the Ca^{2+} site rather than Al^{3+} site. It is suggested that, the co-doping of alkali ions works as charge compensator, induces a lattice distortion and lowers the lattice symmetry

which altogether favors the enhanced emission intensity of ${}^5D_0 \rightarrow {}^7F_2$ transition. The luminescent decay analysis of $\text{CaAl}_2\text{O}_4:\text{Eu}^{3+}$, Li^+ phosphor, monitored at 615 nm under 254 nm excitation, reveals a long decay time, luminescence last over 10 ms. It is also noted that the emission intensity gradually enhances as the ionic radii of the alkali ion decreases, i.e. minimum for K^+ and maximum for Li^+ ion. This has been explained as due to change in ionic radii of alkali ions which influence the local structure around the luminescent center ions. This also influences the spin-orbit couplings and crystal field around Eu^{3+} ions. The excitation spectrum of $\text{CaAl}_2\text{O}_4:\text{Eu}^{3+}$, R^+ (Li, Na and K) shown in Fig 5(a)⁸⁹ depicts a broad band in the range of 200–300 nm which is due to the charge transfer state from O^{2-} to Eu^{3+} ions. The incorporation of alkali ions in the $\text{CaAl}_2\text{O}_4:\text{Eu}^{3+}$ phosphor results in increased CTS band excitation, this might be due to change in Eu–O distances by alkali ions doping.

Tang *et al.*⁹⁰ prepared $\text{Ho}^{3+}/\text{Yb}^{3+}/\text{Li}^+$ co-doped SrAl_2O_4 phosphors and studied the effect of Li^+ ion co-doping on the UC emission of Ho^{3+} ion. At the first step, the concentration of Yb^{3+} ions have been optimized for getting maximum UC emission, which is found to be 0.20 mol fractions. It has been observed that a variation in Yb^{3+} content brings out significant structural changes in the host lattice. The XRD patterns reveal a pure monoclinic-phase of SrAl_2O_4 for Yb^{3+} concentration <0.04 mol fraction, above which two new (minor) phases namely YbAlO_3 and Yb_2O_3 were also identified. On increasing the Yb^{3+} concentration, further the diffraction peaks of SrAl_2O_4 lattice shift towards higher angle which is attributed due to the substitution of Sr^{2+} (1.12 Å) by Yb^{3+} (0.86 Å) having a comparatively smaller ionic radius. The presence of Li^+ at the next step enhances the UC emission intensity, significantly. An enhancement in green UC up to six fold emission was found for Li^+ ion concentration 0.06 (see Fig. 5(b)). This has been proposed both due to charge compensation and grain growth. Due to low melting point of lithium

compound (Li_2CO_3 , 723 °C), it may work as a flux to accelerate grain growth in the SrAl_2O_4 . In a similar study, Chen *et al.*⁹¹ have prepared Ce^{3+} , Eu^{2+} , Li^+ co-doped SrAl_2O_4 phosphor. They found that the doping of Ce^{3+} and Li^+ ion enhances the PL intensity of $\text{SrAl}_2\text{O}_4:\text{Eu}^{2+}$, significantly.

4.4. Effect of alkali ions on PL enhancement of lanthanide ions in perovskite host matrices

Oxides with perovskite structure (chemical formula ABO_3) have large technological importance. They exhibit good piezoelectric, ferroelectric and magnetic properties.^{161, 162} Recently, due to their high dielectric constant, high charge storage capacity, good insulating property, good chemical and physical stability, relatively low phonon energy ($\sim 700 \text{ cm}^{-1}$) these materials are being used for luminescence applications, also. Both UC and DS emission of lanthanide ions doped in perovskite hosts have been reported.^{163, 164} Further, effect of Li^+ ion in enhancing the luminescence efficiency of lanthanides has also been investigated.⁹²⁻⁹⁷ Table 5 briefs the effect of alkali ions on PL enhancement and the possible mechanism for this.

Sun *et al.*⁹² have prepared BaTiO_3 nanocrystals doped with Er^{3+} ion, and further the effect of Li^+ ion co-doping has been investigated to enhance the PL of Er^{3+} . By using 3 mol% Li^+ ion they observed 56 times enhancement (see Fig 6(c)). Authors have attributed this enhancement as being due to a change in crystal field symmetry around Er^{3+} ion, which has been established through XRD measurements. XRD peaks show a gradual shift with addition of Li^+ ion up to 3 mol%, while above 3 mol % doping of Li^+ ion the shift in XRD peak position is not observed. Authors suggest that, since the Li^+ ion has small ionic radius, it can fit in any crystal site, such as substituting either the Ba^{2+} ion or can occupy the interstitial sites as well. Substitution of divalent Ba by Li^+ ion induces oxygen vacancy in the matrix. In both the cases it is apparent that the local crystal field around the Er^{3+} ion will be changed. Another possibility of Li^+ ion doping at Ti^{4+} site

has been discarded in the study as because of the large charge difference between them. Furthermore, it has also been noted that, the addition of Li^+ ion neutralizes OH group concentrations and so decreases the non-radiative channels, also. Thus, the enhanced PL has been attributing to all these factors. In another work on $\text{Er}^{3+}/\text{Yb}^{3+}$ co-doped BaTiO_3 by Chen *et al.*⁹³, time domain studies have also been included to understand the PL enhancement on Li^+ ion co-doping. The decay profiles of the $^4\text{S}_{3/2} \rightarrow ^4\text{I}_{15/2}$ (at 548 nm) and $^4\text{F}_{9/2} \rightarrow ^4\text{I}_{15/2}$ (at 660 nm) transitions have been monitored in different compositions of the doped ions e.g. BaTiO_3 : 1% Er^{3+} and 5% Yb^{3+} and BaTiO_3 : 1% Er^{3+} and 5% Yb^{3+} , 7% Li^+ nanocrystals (see Fig 6(d)). They found that the lifetime of the $^4\text{S}_{3/2}$ state of BaTiO_3 : 1% Er^{3+} and 5% Yb^{3+} , 7% Li^+ nanocrystals (104.4 μs) is longer than BaTiO_3 : 1% Er^{3+} and 5% Yb^{3+} nanocrystals (97.5 μs). This has been attributed due to a decrease in non-radiative channels (OH group concentration) after Li^+ ion doping.

Yang *et al.*^{94, 95} prepared $\text{CaTiO}_3:\text{Pr}^{3+}$ phosphor with different concentrations of Li^+ ion (0.5 to 5.0 wt. %). The maximum PL enhancement (~ 3.5 times) was observed for 1.0 wt.% Li^+ co-doped $\text{CaTiO}_3:\text{Pr}^{3+}$ phosphor. The excitation spectrum observed by monitoring emission at 613 nm (see Fig 6(a)) shows a band at 330 nm which has been assigned to arise due to transition from the valence band to the conduction band, $\text{O}^{2-} (2p) \rightarrow \text{Ti}^{4+} (3d)$; and the other band at 380 nm, has been attributed to the charge transfer (CT) from Pr^{3+} to metal ions, $\text{Pr}^{3+}/\text{Ti}^{4+} \leftrightarrow \text{Pr}^{4+}/\text{Ti}^{3+}$. The emission spectrum recorded on excitation with the charge transfer (CT) band shows high brightness (see Fig. 6(b)). The PL brightness first increases up to 1.0 wt % of Li^+ then start to decrease. The reason behind this has been explored by using XRD and SEM characterization techniques. The XRD analysis reveals that, on addition of Li^+ ion up to 1.0 wt.%, crystallinity increases, while above this, it starts decreasing. Also, for Li^+ concentration more than 2 wt.%

some impurity phase was also detected. The SEM images (see Fig. 6 (e-h)) of $\text{CaTiO}_3:\text{Pr}^{3+}$ doped with different concentrations of Li^+ reveals that the grains of Li-doped $\text{CaTiO}_3:\text{Pr}^{3+}$ phosphors are highly packed and have larger grain size as compared with that of $\text{CaTiO}_3:\text{Pr}^{3+}$. On the basis of these results, it has been concluded that, the high density of packing and improved crystallinity leads to higher oscillating strengths for the optical transitions. Also, the addition of Li^+ ions creates the oxygen vacancies. Due to strong mixing of charge transfer states, the oxygen vacancies act as sensitizer for the energy transfer from host to Pr^{3+} ion. These, altogether is responsible for enhanced photoluminescence of activator ions.

Du *et al.*⁹⁶ prepared Eu^{3+} and Li^+ co-doped CaZrO_3 nanocrystals. The optimum doping level of Eu^{3+} is 5 mol%, above which the PL start decreasing due to concentration quenching. The closed packed structure of CaZrO_3 does not have space to accommodate interstitial atoms. Eu^{3+} ion substitutes Ca^{2+} site. Because of the substitution of Ca^{2+} by Eu^{3+} there would be some charge difference. The addition of 10 mol% of Li^+ ion into CaZrO_3 lattice enhances the PL three times and further increase in Li^+ concentration decreases PL intensity. The enhancement in the PL intensity has been attributed due to the lattice distortion produced after Li^+ ion doping. The lattice distortion reduces the symmetry around Eu^{3+} ions and increases the PL intensity of $^5\text{D}_0 \rightarrow ^7\text{F}_2$ transition. Yu *et al.*⁹⁷ have prepared a series of luminescent materials, $\text{SrZnO}_2:\text{Eu}^{3+}, \text{M}^+$ ($\text{M} = \text{Li}, \text{Na}, \text{K}$). As the ionic radii of Eu^{3+} ions is close to Sr^{2+} than the Zn^{2+} ions it would prefer to occupy the Sr^{2+} site. The substitution of Eu^{3+} for Sr^{2+} , results charge imbalance. The incorporation of alkali metal ions enhanced the PL intensity which has been attributed due to charge compensation.

4.5. Effect of Li⁺ ion on PL enhancement of lanthanide ions in metal oxide nanoparticles

Recent years have witnessed enormous interest in semiconductor nanocrystals due to their potential applications in photocatalysis, solar cells and various other optoelectronic devices.¹⁶⁵⁻¹⁶⁷ Many research groups are working to further enrich the optical and other properties of these semiconductors by combining lanthanide with them. Out of a large number of semiconductor materials available, ZnO, ZnS, TiO₂, MgO and SnO₂ semiconductors have been widely used as host for lanthanide doping due to their large band gap, low phonon energy, excellent physical and chemical stability and environmentally friendly nature.¹⁶⁸⁻¹⁷⁰ These semiconductors are very frequently used in electroluminescent devices. However, due to mismatch in ionic radius of lanthanide ions (usually trivalent for optical applications) and Zn²⁺, Ti⁴⁺, Mg²⁺, Sn⁴⁺ metal ions, it is difficult to accommodate lanthanide ions into the semiconductor matrices. If or otherwise, it creates charge imbalance and vacancy, which affects the luminescence yield significantly. Researchers are using Li⁺ ion to modify the semiconductor host matrices, compensate the charge imbalance so as to improve the luminescence intensity.⁹⁸⁻¹⁰⁵ Table 6 summarizes the role of Li⁺ ion on PL properties of lanthanide ions doped in various semiconductor host matrices.

Gu *et al.*⁹⁸ have prepared Dy³⁺ and Li⁺ co-doped MgO nanocrystals. Li⁺ ion co-doping enhances the emission of Dy³⁺ ions, which has been concluded due to improved crystallinity and grain size and change in symmetry around Dy³⁺ ions. The first conclusion has been drawn on the basis of XRD and TEM measurements, while, ratio of intensity of the magnetic and electric dipole allowed transitions (⁴F_{9/2}→⁶H_{15/2} and ⁴F_{9/2}→⁶H_{13/2} transitions) of Dy³⁺ has been calculated to have an idea about the site symmetry around dysprosium ions. The XRD studies reveal the

pure cubic structure for MgO:Dy³⁺ and Li⁺ co-doped samples. The incorporation of Li⁺ ions increases the crystallinity of MgO nanocrystals. TEM images of MgO crystals exhibit cuboid lamellar morphology having mean particle size ~20 nm, which remains unchanged on addition of Dy³⁺ ions. However, in presence of Li⁺ ion, crystallite size increases to 30–40 nm. They proposed that during the combustion process Li₂O may melt/or react with MgO and Dy₂O₃ and thus forms a eutectic liquid which help to improve the crystallinity. The ⁴F_{9/2}→⁶H_{15/2} and ⁴F_{9/2}→⁶H_{13/2} transitions of Dy³⁺ ion is known as magnetically allowed (hardly varies with the crystal field strength around the dysprosium ion) and forced electric dipole transition (being allowed only at low symmetries with no inversion center), respectively. The ratio of the intensities between the electric dipole and the magnetic dipole gives information about the site symmetry in which the dysprosium ion is situated. Under excitation at 273 nm, asymmetry ratio of Dy³⁺ doped MgO sample is 1.3, whereas, for 20% Li⁺ co-doped sample, it found as 1.5 and also the PL increases four times (see Fig. 7(a)). The variation of the asymmetry ratio indicates change in symmetry and vibrational modes around the Dy³⁺ ions by Li⁺ ions doping.

Zhang *et al.*⁹⁹ have prepared Eu³⁺ and Li⁺ co-doped SnO₂ phosphors. SnO₂ has tetragonal structure (space group of *P42/mnm*), in which Sn atom occupies a slightly distorted octahedral site. The Eu³⁺ ions go into the Sn⁴⁺ site therefore the local environment around Eu³⁺ ions should be of high symmetry, which weakens ⁵D₀→⁷F₂ (613 nm) transition than ⁵D₀→⁷F₁ transition. Li⁺ doping increases the crystallinity and particle size (established through XRD measurements) which induces a remarkable increase of PL intensity. Further, the occupation of Sn⁴⁺ sites by Li⁺ ions would naturally give rise to a considerable number of vacant sites in the oxygen ion array and then expand the lattice to decrease crystal density which may also promote increased PL.

Kallel *et al.*¹⁰⁰ have prepared Y³⁺ and Li⁺ co-doped TiO₂ nanoparticles which have rutile phase. Traces of Y₂Ti₂O₇ anatase are also found for the Y³⁺ doped titania powder. PL studies reveal that incorporation of Li⁺ induces a long lived PL of the order of millisecond time range, with maximum at 724 nm. As the Li⁺ and Y³⁺ concentration increases to 7% or 10%, an increase in emission intensity is observed. Cao *et al.*¹⁰¹ have investigated 1 mol% Er³⁺, 10 mol% Yb³⁺ and 0–20 mol% Li⁺ tri-doped TiO₂ nanocrystals. The XRD pattern reveals that 1Er:TiO₂ has tetragonal rutile phase of TiO₂ with some impurity phase due to Er₂Ti₂O₇. On addition of 10 mol% Yb³⁺ a new phase Yb₂Ti₂O₇ was observed along with rutile TiO₂ and Er₂Ti₂O₇ phases. From the shifts in XRD peak positions of TiO₂, it is revealed that, for low Li⁺ ion concentration (1–2 mol %), it occupy Ti⁴⁺ site, whereas, for higher Li⁺ concentration (5–20 mol %) it goes to interstitial sites. On Yb³⁺ and Li⁺ co-doping, intensity of green and red bands of Er³⁺ increases significantly. This has been attributed to the energy migration between the Er³⁺ and Yb³⁺ as well as the distortion of crystal field symmetry of Er³⁺ for lower concentration of Li⁺, while phase transformation at higher Li⁺ concentration.

Han *et al.*¹⁰² have prepared Er³⁺ doped ZnO nanoparticles. Under 980 nm excitation, this produces strong red emission. On Li⁺ ion co-doping, a luminescent switching between the main red emission band and that green band of Er³⁺ is seen (see Fig 7(b) and (c)). They proposed that the change in UC emission behavior is due to the modification of local crystal field around Er³⁺ ions due to the introduction of Li⁺ ions. Fig. 7(b) shows the XRD patterns of the as prepared and annealed Er³⁺ doped samples. Gu *et al.*¹⁰³ have prepared Dy³⁺-doped ZnO nanocrystals. It is observed that the Li⁺ co-doping in ZnO:Dy³⁺ nanocrystals increases PL by 10 times. They proposed that, since the f-f absorption transitions in lanthanide ions are forbidden, the number of carriers excited through f-f transitions in Dy³⁺ ions is very less in comparison to the excited

through band gap excitation of ZnO. Thus, the improvement in Dy^{3+} emission is mainly due to the radiative recombination of the large amount of trapped carriers excited from ZnO host. The increased recombination probability enhances the emission of Dy^{3+} by energy transfer process. In addition, the incorporation of Li^+ ions can create the oxygen vacancies, which might act as the sensitizer for the energy transfer to the rare earth ion due to the strong mixing of charge transfer states resulting in the highly enhanced luminescence. Further, they have reported reduction of the asymmetry ratio which suggests a change of symmetry and vibrational modes around the luminescent Dy^{3+} centers by Li^+ doping. Bai *et al.*¹⁰⁴ have also studied the role of Li^+ ions on Er^{3+} doped ZnO nanocrystals. They have also observed enhanced UC emission intensity of Er^{3+} ions on Li^+ co-doping. Though the Li^+ ion does not have enough energy to destroy the ErO_6 structure, yet, it may alter the local structure around Er^{3+} which affects the 4f-4f transitions of Er^{3+} ion, which results in UC emission enhancement. Further, Li^+ ion also reduces the OH⁻ group concentration, which is another reason for the UC emission intensities enhancement.

Liu *et al.*¹⁰⁵ have demonstrated the UC emission in Er^{3+} , Yb^{3+} and Li^+ tri-doped ZrO_2 nanocrystals. The incorporation of Li^+ ions increases the emission intensities of green and red bands of Er^{3+} by a factor of 1.93 and 1.65, respectively. The XRD pattern reveals that, Er^{3+} doped ZrO_2 samples have both the tetragonal and monoclinic phases. $\text{Yb}^{3+}/\text{Er}^{3+}$ co-doping increases the formation of the tetragonal phase in the sample. Further, the incorporation of Li^+ suppressed the tetragonal phase in $\text{Yb}^{3+}/\text{Er}^{3+}$ doped ZrO_2 sample (Fig. 7d)). Further, on Li^+ doping the slopes of the excitation power versus UC emission intensities curve decreases (see Fig 8(e)), which suggests that Li^+ ions can tailor the local structure of the host lattice and thus can improve energy transfer processes from Yb^{3+} to Er^{3+} ions.

4.6. Effect of alkali ions on UC emission of lanthanide ions in fluoride host matrices

Fluoride host matrices, particularly NaYF₄ and NaGdF₄, are known to be excellent host for UC studies.^{54, 106} Due to their similar ionic radius, Na⁺ and RE³⁺ ions occupy the same sites in the hexagonal NaYF₄ lattice. These host matrices possess low phonon energies which is an essential requirement for getting efficient UC emission. They show higher chemical stability than other halides (chloride, bromide).^{54, 106} The crystal structure of these matrices highly influences the UC properties, and crystal structure is quite sensitive to the alkali ions present in the crystal. So, it is interesting to study the effect of alkali ions on the UC properties of fluoride host matrices.

Mao *et al.*¹⁰⁷ have studied the effect of alkali ions (Li⁺ and K⁺) on crystal structure and UC emission of NaYF₄:Yb/Er crystals. It was observed that the Li⁺ ion co-doping in the NaYF₄:Yb/Er crystals affects the morphologies to a greater extent and significant changes from rod like shape to disk shape and finally to polyhedron structure is attained. However, K⁺ ion co-doped NaYF₄:Yb/Er crystals do not show any change in morphology and it almost maintains the rodlike shape throughout (see schemes (a) and (c) in Fig 8). The crystal structure analysis further reveals that, not only the surface morphology, but phase transition from β-hexagonal to tetragonal (LiYF₄) in Li_xNa_{1-x}YF₄ crystals is also initiated at x = 0.5, whereas, the phase of K_yNa_{1-y}YF₄ remains stable up to y=0.85. The UC emission studies show that as the Li⁺ content increases in the crystal UC emission intensity decreases, whereas, the UC emission intensity of NaYF₄:Yb/Er crystals increases (K_{0.7}Na_{0.3}YF₄:Yb,Er crystal shows 8 and 7 times enhancement in green and red UC emission, respectively) when K⁺ ions are introduced in the crystal (see Fig 8 (b) and (c)). The change in UC emission is related to the change in crystal structure, surface morphology, and distance between alkali and fluorine atoms. In Li⁺ doped crystal, Li-F distance will be higher than Na-F distance which can intensify the interaction between F⁻ and Er³⁺ in

the crystal lattice which may enhance the phonon energy of Er^{3+} ions. On the other hand, substitution of Na^+ ions with K^+ ions in the lattice reduces the inter-quenching of Er^+ , decreases the local crystal field symmetry which increases UC intensity. In a similar work, Dou and Zhang¹¹⁴ have also studied effect of Li^+ and K^+ ions doping on crystal structure and UC emission behavior of $\text{NaYF}_4:\text{Yb}/\text{Er}$. The phase transition in $\text{NaYF}_4:\text{Yb}/\text{Er}$ crystal, has also been observed by Dou and Zhang [Ref 10] on Li^+ ion doping, but instead of hexagonal to tetragonal phase transition, as observed by Mao *et al.*¹⁰⁷, they observed hexagonal to cubic phase transition. The UC studies reveal that the intensity ratios between the blue, green, and red emission peaks changes on Li^+ and K^+ doping in the crystal. They have proposed that the Li^+ or K^+ doping will slightly change the size of the unit cell in the crystal and then to change the Yb-Er distance which can influence energy transfer process. On the other hand, the higher concentration of K^+ ions in the crystal causes formation of a new K_2NaYF_6 phase. The coordination number of RE is 9 in hexagonal phase, 8 in cubic phase and 6 in K_2NaYF_6 phase. This suggests that K_2NaYF_6 phase is less stable than cubic and hexagonal phases. Further, Misiak *et al.*¹¹⁰ have shown that Li^+ doping in the cubic $\text{NaYF}_4:\text{Yb}^{3+}/\text{Tm}^{3+}$ colloidal crystals, significantly reduces the concentration quenching. Interestingly, the initial UC emission intensity decreases first, and then starts increasing. This might be due to the fact that initially Li^+ ions substitutes the Na^+ ions in the lattice, while further increase in the Li^+ ion concentration results the occupancy of Li^+ ions in the interstitial sites, which results increase in the crystal size. Further, substitution of Na^+ by Li^+ introduces distortion in the lattice which prevents concentration quenching.

Similar to the NaYF_4 , co-doping of alkalis Li^+ bring out significant changes in crystal structure and optical properties are greatly improved. Cheng *et al.*¹¹¹ have studied effect of Li^+ ions on UC emission of $\beta\text{-NaGdF}_4:\text{Yb}^{3+}/\text{Er}^{3+}$ nanoparticles. It is found that the presence Li^+ ions

in the crystal enhanced UC emission drastically (nanoparticles doped with 7 mol % Li^+ ions show 47 and 23 times enhancement in green and red UC emission peaks, respectively). The enhanced UC emission is attributed to the distortion of the local asymmetry around Er^{3+} ions. The presence of Li^+ in the nanoparticles also helps in the growth of crystal, which is proved by XRD studies. Another contributing factor to the enhanced UC is the increased lifetime of the $^4\text{S}_{3/2}$ state of $\text{NaGdF}_4: \text{Yb}^{3+}/\text{Er}^{3+}$ NPs in the Li^+ ions doped crystals (see Fig. 9) which causes increased population in $^4\text{S}_{3/2}$ state resulting enhanced green emission. Furthermore, the presence of Li^+ also increases paramagnetic behavior of the nanoparticles. This attributed to the increase in Gd^{3+} molar concentration in NaGdF_4 resulting due to introduction of Li^+ ions. Zhang *et al.*¹⁰⁹ have also studied effect of Li^+ ions on UC emission behavior of $\text{NaYbF}_4:\text{Er}$ microcrystals. Interesting, they observed a blue shift in UC emission bands. The XRD studies show hexagonal to tetragonal phase transformation on Li^+ co-doping. In LiYbF_4 crystal, each Yb^{3+} ion is coordinated with eight F^- ions (forming the YbF_8 polyhedral units) and each Li^+ ion is coordinated with four F^- ions (forming the LiF_4 tetrahedral units). The crystallographic point site symmetry with S_4 symmetry in LiYbF_4 is higher than that of NaYbF_4 with D_{2d} symmetry. This results a more symmetrical distribution of electronic density and a weakened polarization effect of the local environment in LiYbF_4 causes a blue shift in UC bands. Guo *et al.*¹¹³ have studied effect of Li^+ ions on UC emission behavior of $\text{Lu}_6\text{O}_5\text{F}_8: \text{Yb}^{3+}/\text{Er}^{3+}$ nanoparticles. They have studied UC, DC and CL properties of the materials and all these increases in the presence of Li^+ ions. They proposed that increased luminescence properties is due to the increased crystallinity (by flux action of Li), decreased absorption bands of the surface contaminants (OH and CO groups) and distorted local symmetry around the Er^{3+} ions. Yin *et al.*¹⁰⁸ have studied the effect of Li^+ on UC emission behavior of $\text{GdF}_3:\text{Yb}, \text{Er}$ nanoparticles. In $\text{GdF}_3:\text{Yb}, \text{Er}$ nanoparticles, the

intensity of UC emission in the red region is higher than that in the green region which results a bright yellow emission even observable by the naked eye. On Li^+ doping (0 to 5, 10, and 25 mol%) the green emission intensity gradually decreases and the red emission is enhanced (see Fig 9 (c-g)). This attributed to the change in local crystal field around Er^{3+} ions in the presence of Li^+ ions in the $\text{GdF}_3:\text{Yb,Er}$ host lattice.

Thus in summary, it is pointed out that, alkalis in fluorides and similar hosts effectively modifies the crystal structure and affects the surface morphology, phase, particle size, crystallinity, *etc.* By this way the crystal field around lanthanide ion is favorably changed. Not only this, the doping of alkalis makes a significant change in critical separation between lanthanide ions, lanthanide-alkali ions, lanthanide-fluorine ions, lanthanide activator and sensitizers, *etc.*, due to which energy transfer processes becomes effective giving rise to an increase in the UC emission. A change in the different component of the emission viz. blue, green and red varies systematically which creates opportunity for color tunability also. Above to all this, a specific blue shift is also observed, which is peculiar in this host. Some interesting observations, although beyond the scope of this study, e.g. increase in the paramagnetic behavior could of very useful for related readers.

4.7. Effect of alkali ions on luminescence enhancement of lanthanide ions in miscellaneous host matrices

The preceding sections described the role of alkali ions, especially Li^+ , on the luminescence properties in some well known host matrices viz. Y_2O_3 and Gd_2O_3 , ABO_4 type of compounds, strontium and calcium aluminates, perovskite, oxide nanoparticles and fluoride host matrices. In addition to these, there are several other host matrices viz. $\text{Ba}_2\text{GdNbO}_6$: $\text{Eu}^{3+}/\text{Dy}^{3+}$, Li^+ ¹¹⁵, $\text{BaZn}_2(\text{PO}_4)_2$: Sm^{3+} , R^+ ($\text{R} = \text{Li, Na, K}$)¹¹⁶, $\text{Ca}_3\text{B}_2\text{O}_6$: Dy^{3+} , Li^+ ¹¹⁷, CaSO_4 : $\text{Tm}^{3+}/\text{Dy}^{3+}$, Li^+

¹¹⁸, (Y, Gd)BO₃: Tb³⁺, Li⁺ ¹¹⁹, YNbTiO₆: Eu³⁺, Li⁺ ¹²⁰, YBO₃: Eu³⁺, Li⁺ ¹²¹, Zn₂SiO₄:Yb³⁺, Er³⁺, Li⁺/Bi³⁺ ¹²², SrB₄O₇: Eu²⁺, Li⁺ ¹²³, Lu₂SiO₅: Ce, Li⁺ ¹²⁵, Y₂MoO₆:Eu³⁺, Li⁺ ¹²⁶, NaSrBO₃:Tb³⁺, Li⁺ ¹²⁷, Sr₂SiO₄:Eu³⁺, (Li⁺, Na⁺, K⁺)¹²⁹, CaSnO₃:Tb³⁺ (Li⁺, Na⁺, K⁺)¹³¹, Gd₆MoO₁₂: Li⁺/Ln³⁺ ¹³², Y₂SiO₅:Pr³⁺, Li⁺ ¹³³, Y₂Zr₂O₇:Dy³⁺, Li⁺ ¹³⁴, Li_xCa_{1-2x}Eu_xSi_yMo_{1-y}O₄ ¹³⁶, Ca₂BO₃Cl:Sm³⁺ (Li⁺,Na⁺,K⁺) ¹³⁹ and CaSi₂O₂N₂:Eu²⁺, Dy³⁺, Li⁺ ¹⁴⁰, *etc.* in which the role of Li⁺ on luminescence properties have also been investigated. Table 8 gives brief information about these and also outline various possible mechanism involved in the PL enhancement. It is basically due to increased crystallinity, grain size, charge compensation, change in local crystal field around the lanthanide ions, *etc.* All these mechanisms are discussed in the preceding sections in context of other well known matrices, so here we are not discussing it again.

5. Conclusions

The review was planned with prime objective to explore the effect of Li⁺ ion co-doping on the PL of lanthanide ions doped in different host matrices, and also to highlight various contributing factors which plays an important roles. The follow up of the literature reviewed so far in this article unanimously depicts that the co-doping of Li⁺ ion up to a certain concentration in lanthanide doped phosphors enhances the luminescence (both for UC and DC based emission) of lanthanide ions considerably.

The possible explanation for the enhanced PL intensity of the lanthanide ions in the presence of Li⁺ ions can be summarized as follows. When Li⁺ ion is introduced in any matrix, because of its smaller ionic radius, it can either substitute the cation of the matrix or can occupy interstitial sites of the matrix, which usually depends on the concentration of doped alkali. As the Li⁺ ion concentration increases, the possibility for occupying the interstitial sites increases which

distorts matrix, significantly. In few host, changes even in phase and crystal structure are also marked. The change in crystal structure can also change the occupancy site of the lanthanide ions. Also, due to the lower melting temperature of the Li it can work as a flux and increase the crystallinity and the grain size of the materials. In addition, it is also found that Li^+ ion decreases the concentration of the inorganic/organic groups which work as a non-radiative channels and causes to decrease the PL intensity. Further, when trivalent lanthanide ion replaces divalent cation it produces charge imbalance in the matrix which can be compensated by using alkali ions. All these favors luminescence enhancement of the lanthanide ions. In case of Ce^{3+} and Eu^{2+} ions, by changing the local crystal fields around the activator ions, it can also be used for tuning the color of the luminescence materials. Furthermore, in fluoride host matrices, co-doping of Li^+ causes a change in separation between lanthanide ions, lanthanide-alkali ions, lanthanide-fluorine ions, lanthanide activator and sensitizers, *etc.*, which strongly influences the energy transfer processes. Thus, it can be concluded that the Li^+ ions (alkali ions) modifies host matrices in many ways which favors radiative transitions, causing enhancement in the luminescence intensity. Since, the review provides in-depth case studies for various hosts, and describes the effect of various matrix parameters (e.g. crystal structure, crystallinity, grain size, surface morphology, quenching entities, *etc.*) on PL, therefore, it could also be useful as input for designing of various novel lanthanide doped luminescent materials.

Effect of co-doping of Li^+ ion have been used for almost all different types of luminescence mechanisms including photoluminescence/downshifting, upconversion, thermo-luminescence/persistent emission, cathodo-luminescence, *etc.* However, its use for one of the most important class of emissions, i.e. quantum-cutting, is still lagging and has strong scope for future studies.

Acknowledgements

S. K. Singh thankfully acknowledges the financial support by Department of Science and Technology, New Delhi, India in the form of INSPIRE Faculty Award [IFA12-PH-21]. A. K. Singh acknowledges financial support by UGC, New Delhi, India (Dr. D. S. Kothari postdoctoral fellowship (No. F. 4-2/2006 (BSR)/13-906/2013 (BSR)) from April 2013 to February 2014) and UNAM, Mexico (DGAPA, started from March 2014) in the form of postdoctoral fellowships.

References

1. J. R. Lakowicz, *Principles of Fluorescence Spectroscopy*, Springer, Singapore, 2002.
2. C. R. Ronda, *Luminescence*, Wiley-VCH, Germany, 2008.
3. A. Kitai, *Luminescent Materials and Applications*, John Wiley & Sons Ltd., England, 2008.
4. B. Yan, *RSC Adv.*, 2012, **2**, 9304-9324.
5. O. S. Wolfbeis, *Lanthanide Luminescence*, Springer, New York, 2011.
6. B. G. Wybourne, *Optical Spectroscopy of Lanthanides*, CRC Press, Taylor and Francis, Boca Raton, USA, 2007.
7. Zimmermann, S. Hesse, H. von Seggern, M. Fuchs and W. Knüpfner, *J. Appl. Phys.*, 2007, **101**, 113711-113717.
8. J. Liu, J. Sun and C. Shi, *Mater. Lett.*, 2006, **60**, 2830-2833.
9. Y. Kojima, K. Aoyagi and T. Yasue, *J. of Lumin.*, 2005, **115**, 13-18.
10. Z. Hao, X. Zhang, Y. Luo, L. Zhang, H. Zhao and J. Zhang, *J. of Lumin.*, 2013, **140**, 78-81.
11. L. Chen, Y. Zhang, F. Liu, A. Luo, Z. Chen, Y. Jiang, S. Chen, R. S. Liu, *Mater. Res. Bull.*, 2012, **47**, 4071-4075.
12. B. K. Grandhe, V. R. Bandi, K. Jang, H. S. Lee, D. S. Shin, S. S. Yi, J. H. Jeong, *Ceram. Intern.*, 2012, **38**, 6273-6279.
13. X. Zhang, and H. J. Seo, *Phys. Status Solidi A*, 2010, **207**, 428-431.
14. C. Shen, K. Li, Y. Yang, *SPIE-OSA-IEEE*, 2009, 7635, 76350K-1.
15. L. Jia, M. Gu, X. Liu, S. Huang, B. Liu, and C. Ni, *IEEE Trans Nucl. Sci.*, 2010, **57**, 1268-1271.
16. P. Zhu, T. Huang, X. Wang, H. Li, and Z. Sun, *Adv. Mater. Res.*, 2013, **690-693**, 555-558.

17. X. M. Wang, X. Zhang, S. Ye and X. P. Jing, *Dalton Trans.*, 2013, **42**, 5167-5173.
18. H. S. Jang, H. Yang, S. W. Kim, J. Y. Han, S. G. Lee, and D. Y. Jeon. *Adv. Mater.* 2008, **20**, 2696–2702.
19. X. M. Wang, C. H. Wang, X. J. Kuang, R. Q. Zou, Y. X. Wang, and X. P. Jing, *Inorg. Chem.*, 2012, **51**, 3540–3547.
20. W. Su, M. He, J. Xing, Y. Zhong and Z. Li, *RSC Adv.*, 2013, **3**, 25970-25975.
21. Y. Dwivedi, A. K. Singh, R. Prakash and S. B. Rai, *J. Lumin.*, 2011, **131**, 2451-2456.
22. S. V. Eliseeva and J. G. Bünzli, *Chem. Soc. Rev.*, 2010, **39**, 189-227.
23. L. Sun, Y. Qiu, T. Liu, H. Peng, W. Deng, Z. Wang and L. Shi, *RSC Adv.*, 2013, **3**, 26367-26375.
24. A. K. Singh, S. K. Singh, P. Kumar, B. K. Gupta, R. Prakash and S. B. Rai, *Sci. Adv. Mater.*, 2014, **6**, 405-412.
25. L. D. Carlos, R. A. S. Ferreira, V. de Z. Bermudez and S. J. L. Ribeiro, *Adv. Mater.*, 2009, **5**, 509-534.
26. R. K. Verma, A. K. Singh, D. K. Rai and S. B. Rai, *Mat. Chem. Phys.*, 2012, **135**, 298-303.
27. S. Aime, M. Fasano and E. Terreno, *Chem. Soc. Rev.*, 1998, **27**, 19-29.
28. G. F. Sá, O. L. Malta, C. M. Donegá, A. M. Simas, R. L. Longo, P. A. Santa-Cruz and E. F. Silva, *Coord. Chem. Rev.*, 2000, **196**, 165-195.
29. A. K. Singh, S. K. Singh, B. K. Gupta, R. Prakash and S. B. Rai, *Dalton Trans.*, 2013, **42**, 1065-1072.
30. F. Zheng, J. Zhang and S. Feng, *RSC Adv.*, 2013, **3**, 9957-9964.
31. X. Huang, S. Han, W. Huang, and X. Liu, *Chem. Soc. Rev.*, 2013, **42**, 173-201.
32. B. M. Ende, L. Aarts and A. Meijerink, *Phys. Chem. Chem. Phys.*, 2009, **11**, 11081-11095.
33. S. K. Singh, A. K. Singh and S. B. Rai, *Nanotechnology*, 2011, **22**, 275703-275712.
34. F. Wang, D. Banerjee, Y. Liu, X. Chen and X. Liu, *Analyst*, 2010, **135**, 1839–1854.
35. Y. Liu, D. Tu, H. Zhu, R. Li, W. Luo and X. Chen, *Adv. Mater.*, 2010, **22**, 3266–3271.
36. T. Forster, *Discuss. Faraday Soc.* 1959, **27**, 7–17.
37. http://chemwiki.ucdavis.edu/Theoretical_Chemistry/Fundamentals/Dexter_Energy_Transfer

38. A. K. Singh, S. K. Singh, H. Mishra, R. Prakash and S. B. Rai, *J. Phys. Chem. B*, 2010, **114**, 13042-13051.
39. W. F. Sager, N. Filipescu and F. A. Serafin, *J. Phys. Chem.* 1965, **69**, 1092-1100.
40. A K. Singh, S.K. Singh, R. Prakash and S.B. Rai, *Chem. Phys. Lett.*, 2010, **485**, 309-314.
41. F. Wang, R. Deng, J. Wang, Q. Wang, Y. Han, H. Zhu, X. Chen and X. Liu, *Nature Mater.*, 2011, **10**, 968–973.
42. J. Georges, *Analyst*, 1993, **118**, 1481-1486.
43. C. Zhong, P. Yang, X. Li, C. Li, D. Wang, S. Gai and J. Lin, *RSC Advances*, 2012, **2**, 3194–3197.
44. S. K. Singh, K. Kumar, S. B. Rai, *Appl Phys B*, 2009, **94**, 165-173
45. M. M. Saboktakin, X. Ye, S. Ju Oh, S. H. Hong, A. T. Fafarman, U. K. Chettiar, M. M. N. Engheta, C. B. Murray and C. R. Kagan, *ACS Nano*, 2012, **6**, 8758-8766.
46. Y. Wang, L. Xie and H. Zhang, *J. Appl. Phys.*, 2009, **105**, 023528-023532.
47. N. Kodama and Y. Watanabe, *Appl. Phys. Lett.*, 2004, **84**, 4141-4143.
48. B. Moine, L. Beauzamy, P. Gredin, G. Wallez and J. Labeguerie, *Optical. Mater.*, 2008, **30**, 1083–1087.
49. Q. Y. Zhang and X. Y. Huang, *Prog. Mater. Sci.*, 2010, **55**, 353–427.
50. J. H. Yu, X. Liu, K. E. Kweon, J. Joo, J. Park, K. T. Ko, D. W. Lee, S. Shen, K. Tivakornsasithorn, J. S. Son, J. H. Park, Y. W. Kim, G. S. Hwang, M. Dobrowolska, J. K. Furdyna and T. Hyeon, *Nature Mater.*, 2010, **9**, 47-53.
51. K. Mishra, S. K. Singh, A.K. Singh and S.B. Rai, *Mat. Res. Bull.*, 2012, **47**, 1339-1344.
52. J. C. G. Bünzli and C. Piguet, *Chem. Soc. Rev.*, 2005, **34**, 1048-1077.
53. K. Binnemans, *Chem. Rev.*, 2009, **109**, 4283–4374.
54. F. Wang, J. Wang and X. Liu, *Angew. Chem. Int. Ed.* 2010, **49**, 7456 –7460.
55. P. Dorenbos, *J. Lumin.*, 2003, **104**, 239-260.
56. J. H. Jeong, H. K. Yang, B. K. Moon, J. S. Bae, S. S. Yi., H. Choi, J. H. Kim, S. T. Chung, *Optical Mater.*, 2006, **28**, 693–697.
57. S. H. Shin, J. H. Kang, D. Y. Jeon, D. S. Zang, *J. Luminesc.*, 2005, **114**, 275–280.
58. N. Dhananjayaa, H. Nagabhushana, B. M. Nagabhushana, B. Rudraswamy, C. Shivakumara, R. P. S. Chakradhar, *J. Alloys and Comp.*, 2011, **509**, 2368–2374.

59. S. S. Yi, J. S. Bae, K. S. Shim, J. H. Jeong, J. C. Park, P. H. Holloway, *Appl. Phys. Lett.*, 2004, **84**, 353.
60. Q. Sun, H. Zhao, X. Chen, F. Wang, W. Cai, Z. Jiang, *Mater. Chem. and Phys.*, 2010, **123**, 806–810.
61. Y. Jia, Y. Song, Y. Bai, Y. Wang, *Luminescence*, 2010, **26**, 259–263.
62. T. Fan, Q. Zhang, Z. Jiang, *Optics Commun.*, 2011, **284**, 1594–1597.
63. H. Liang, G. Chen, H. Liu, Z. Zhang, *J. Luminesc.*, 2009, **129**, 197–202.
64. G. Chen, H. Liu, H. Liang, G. Somesfalean, Z. Zhang, *J. Phys. Chem. C* 2008, **112**, 12030–12036
65. Y. Bai, K. Yang, Y. Wang, X. Zhang, Y. Song, *Optics Commun.* 2008, **281**, 2930–2932.
66. G. Y. Chen, H. C. Liu, G. Somesfalean, Y. Q. Sheng, H. J. Liang, Z. G. Zhang, Q. Sun, F. P. Wang, *Appl. Phys. Lett.* 2008, **92**, 113114-113116.
67. G. Y. Chen, H. C. Liu, H. J. Liang, G. Somesfalean, Z. G. Zhang, *Solid State Commun.* 2008, **148**, 96–100
68. S. S. Yi, K. S. Shim, H. K. Yang, B. K. Moon, B. C. Choi, J. H. Jeong, J. H. Kim and J. S. Bae, *Appl. Phys. A*, 2007, **87**, 667-271.
69. L. Sun, C. Qian, C. Liao, X. Wang and C. Yan, *Solid State Commun.*, 2001, **119**, 393-396.
70. H. Liang, Y. Zheng, G. Chen, L. Wu, Z. Zhang, W. Cao, *J. Alloys and Comp.*, 2011, **509**, 409–413.
71. D. Li, Y. Wang, X. Zhang, H. Dong, L. Liu, G. Shi and Y. Song, *J. Appl. Phys.*, 2012, **112**, 094701-094705.
72. T. Fan, Q. Zhang, Z. Jiang, *Optics Commun.*, 2011, **284**, 249–251.
73. T. Fan, Q. Zhang, and Z. Jiang, *J. Opt.*, 2011, **13**, 015001-015004.
74. K. Mishra, S. K. Singh, A. K. Singh and S. B. Rai, *Mat. Res. Bull.*, 2013, **48**, 4307–4313.
75. D. Wei, Y. Huang, S. Zhang, Y.M. Yu and H.J. Seo, *Appl Phys B*, 2012, **108**, 447–453.
76. J. H. Chung, J. H. Ryu, J. W. Eun, J. H. Lee, S. Y. Lee, T. H. Heo and K. B. Shim, *Mat. Chem. and Phys.*, 2012, **134**, 695-699.
77. G. Li, J. Guoqi, Y. Baozhu, L. Xu, J. Litao, Y. Zhiping and F. Guangsheng, *J. Rare Earths*, 2011, **29**, 540-543.
78. X. Li, Z. Yang, L. Guan, J. Guo, Y. Wang and Q. Guo, *J. Alloys and Comp*, 2009, **478**, 684–686.

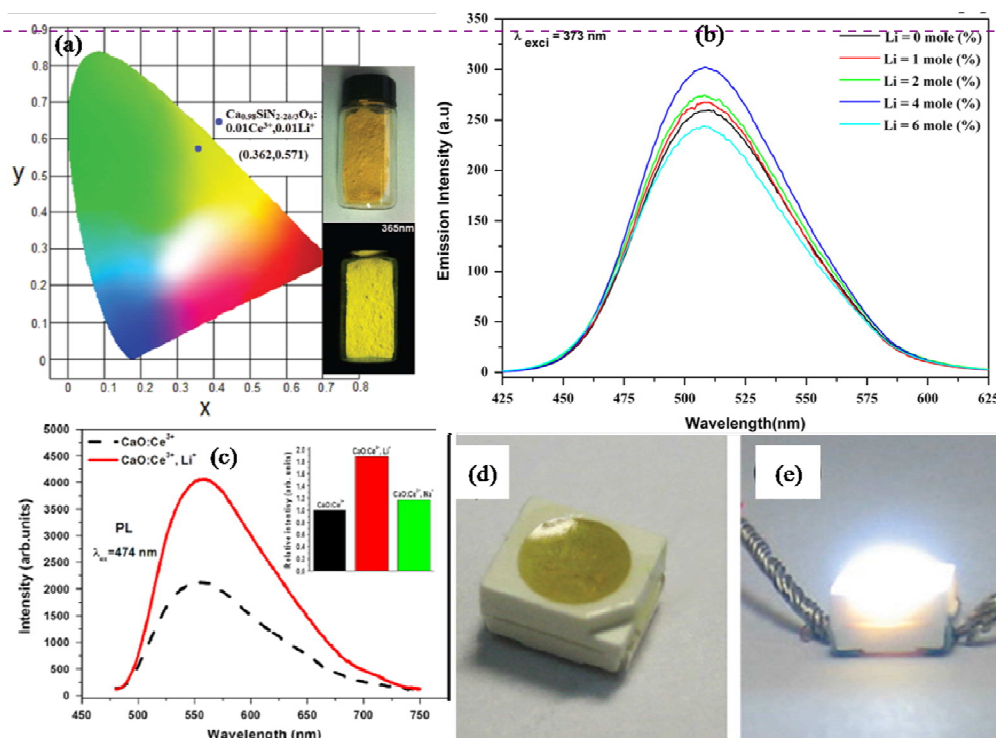
79. W. Li and J. Lee, *J. Phys. Chem. C* 2008, **112**, 11679–11684.
80. S. W. Park, H. K. Yang, J. W. Chung, B. K. Moon, B. C. Choi and J. H. Jeong, *J. Korean Phys. Soc.*, 2010, **57**, 1764-1768.
81. A. K. Parchur, A. I. Prasad, S. B. Rai and R. S. Ningthoujam, *Dalton Trans.*, 2012, **41**, 13810-13814.
82. J. Huang, R. Gao, Z. Lu, D. Qian, W. Li, B. Huang and X. He, *Optical Mater.* 2010, **32**, 857–861.
83. A. K. Parchur and R. S. Ningthoujam, *RSC Advances*, 2012, **2**, 10854–10858.
84. A. K. Parchur, A. I. Prasad, S. B. Rai, R. Tewari, R. K. Sahu, G. S. Okram, R. A. Singh, and R. S. Ningthoujam, *AIP Advances*, 2012, **2**, 032119-032135.
85. A. K. Parchur and R. S. Ningthoujam *RSC Advances*, 2012, **2**, 10859–10868.
86. H. K. Yang, H. Choi, B. K. Moon, B. C. Choi, J. H. Jeong, J. H. Kim and K. H. Kim, *Solid State Sci.*, 2010, **12**, 1445-1448.
87. H. K. Yang, K. S. Shim, B. K. Moon, B. C. Choi, J. H. Jeong., S. S. Yi and J. H. Kim, *Thin Solid Films*, 2008, **516**, 5577–5581.
88. X. Luo and W. Cao, *J. Mater. Res.*, 2008, **23**, 2078-2083.
89. L. Guanghuan, L. Tao, S. Yanhua, G. Guimei, X. Jijing, A. Baichao, G. Shucui and H. Guangyan, *J. Rare Earths*, 2010, **28**, 22-25.
90. M. Tang, X. Wang, D. Peng, W. Wang, H. Sun and X. Yao, *J. Alloys and Comp.*, 2012, **529**, 49– 51.
91. L. Chen, Y. Zhang, F. Liu, A. Luo, Z. Chen, Y. Jiang, S. Chen and R. S. Liu, *Mat. Res. Bull.*, 2012, **47**, 4071–4075.
92. Q. Sun, X. Chen, Z. Liu, F. Wang, Z. Jiang, C. Wang, *J. Alloys and Comp.*, 2011, **509**, 5336–5340.
93. X. Chen, Z. Liu, Q. Sun, M. Ye and F. Wang, *Optics Commun.*, 2011, **284**, 2046–2049.
94. H. K. Yang, J. W. Chung, B. K. Moon, B. C. Choi, J. H. Jeong, J. S. Bae and K. H. Kim, *Solid State Sci.* 2011, **13**, 1420-1423.
95. H. K. Yang, J. W. Chung, B. K. Moon, B. C. Choi, J. H. Jeong and Kwang and H. Kim, *J. Phys. D: Appl. Phys.*, 2009, **42**, 085411-085415.
96. Q. Du, G. Zhou, J. Zhou, H. Zhou, *J. Lumin.*, 2013, **137**, 83–87.
97. X. Yu, X. Xu, C. Zhou, J. Tang, X. Peng, S. Yang, *Mat. Res. Bull.*, 2006, **41**, 1578–1583.

98. F. Gu, C. Li, H. Cao, W. Shao, Y. Hu, J. Chen and A. Chen, *J. Alloys and Comp.*, 2008, **453**, 361–365.
99. H. Zhang, X. Fu, S. Niu, G. Sun and Q. Xin, *J. Lumines*, 2005, **115**, 7–12.
100. W. Kallel, S. Bouattour, L.F. Vieira Ferreira and A.M. Botelho do Rego, *Mater. Chem. Phys.*, 2009, **114**, 304–308.
101. B. S. Cao, Y. Y. He, Z. Q. Feng, M. Song and B. Dong, *Optics Commun.*, 2011, **284**, 3311–3314.
102. H. L. Han, L. W. Yang, Y. X. Liu, Y. Y. Zhang, Q. B. Yang, *Optical Mater.*, 2008, **31**, 338–341.
103. F. Gu, S. F. Wang, M. K. Lu, G. J. Zhou, D. Xu, and D. R. Yuan, *Langmuir*, 2004, **20**, 3528–3531.
104. Y. Bai, Y. Wang, K. Yang, X. Zhang, G. Peng, Y. Song, Z. Pan and C. H. Wang, *J. Phys. Chem. C*, 2008, **112**, 12259–12263.
105. L. Liu, Y. Wang, X. Zhang, K. Yang, Y. Bai, C. Huang, W. Han, C. Li and Y. Song, *Optical Mater.*, 2011, **33** 1234–1238.
106. Q. Su, S. Han, X. Xie, H. Zhu, H. Chen, C. K. Chen, R. S. Liu, X. Chen, F. Wang and X. Liu, *J. Am. Chem. Soc.*, 2012, **134**, 20849–20857.
107. C. Mao, X. Yang and L. Zhao, *Chem. Eng. J.*, 2013, **229**, 429–435.
108. W. Yin, L. Zhao, L. Zhou, Z. Gu, X. Liu, G. Tian, S. Jin, L. Yan, W. Ren, G. Xing and Y. Zhao, *Chem. Eur. J.*, 2012, **18**, 9239 – 9245.
109. X. Zhang, M. Wang, J. Ding, D. Gao, Y. Shia and X. Song, *CrystEngComm*, 2012, **14**, 8357–8360.
110. M. Misiak, B. Cichy, A. Bednarkiewicz, W. Stręk, *J. of Lumin.*, 2014, **145**, 956–962.
111. Q. Cheng, J. Sui, and W Cai, *Nanoscale*, 2012, **4**, 779–784.
112. L. Guo, Y. Wang, Z. Zou, B. Wang, X. Guo, L. Han and W. Zeng, *J. Mater. Chem. C*, 2014, **2**, 2765–2772.
113. L. Guo, Y. Wang, Y. Wang, J. Zhang, P. Dong and W. Zeng, *Nanoscale*, 2013, **5**, 2491–2504.
114. Q. Dou and Y. Zhang, *Langmuir*, 2011, **27**, 13236–13241.
115. C. C. Yu, X.M. Liu, M. Yu, C.K. Lin, C.X. Li, H. Wang and J. Lin, *J. Solid State Chem.*, 2007, **180**, 3058–3065.

116. Z. Wang, P. Li, Z. Yang and Q. Guo, *J. Lumines.*, 2012, **132**, 1944–1948.
117. X. Sun, J. Zhang, X. Liu and L. Lin, *Ceram. Intern.*, 2012, **38**, 1065–1070.
118. Y. Wang, N. Can and P. D. Townsend, *J. Lumines.*, 2011, **131**, 1864–1868.
119. X. Huibing, Z. Weidong, W. Xiaofan, L. Ronghui, HU Yunsheng and X. Tian, *J. Rare Earths*, 2010, **28**, 701-704.
120. Q. Ma, Y. Zhou, A. Zhang, M. Lu, G. Zhou and C. Li, *Solid State Sci.*, 2009, **11**, 1124–1130.
121. D. Jin, J. Yang, X. Miao, L. Wang, S. Guo, N. Wang and L. Wang, *Mater. Lett.*, 2012, **79**, 225–228.
122. L. Jiang, S. Xiao, X. Yang, J. Ding and K. Dong, *Appl Phys B*, 2012, **107**, 477–481.
123. Z. Jiao, S. Li, Q. Yan, X. Wang, D. Shen, *J. Phys. Chem. Solids*, 2011, **72**, 252–255.
124. J. Huang, J. Xu, H. Luo, X. Yu and Y. Li, *Inorg. Chem.*, 2011, **50**, 11487–11492.
125. L. Jia, M. Gu, X. Liu, S. Huang, B. Liu and C. Ni, *IEEE Trans. Nucl. Sci.*, 2010, **57**, 1268–1271.
126. H. Jin, H Wu and L. Tian, *J. Lumin.*, 2012, **132**, 1188–1191.
127. F. Yang, Y. Liang, Y. Lan, W. Gao, M. Liu, X. Li, W. Huang, Y. Li and Z. Xia, *Mater. Lett.*, 2012, **83**, 59–61.
128. R. Wang, J. Xu and C. Chen, *Mater Lett.*, 2012, **68**, 307–309.
129. H. Liu, Y. Hao, H. Wang, J. Zhao, P. Huang and B. Xu, *J. Lumin.*, 2011, **131**, 2422–2426.
130. H. Yanlin, J. Kiwan, W. Xigang and J. Chuanfang, *J. Rare Earths*, 2008, **26**, 490-494.
131. Z. Liang, J. Zhang, J. Sun, X. Li, L. Cheng, H. Zhong, S. Fu, Y. Tian and B. Chen, *Physica B*, 2013, **412**, 36–40.
132. J. Sun, B. Xue and H. Du, *Optics Commun.*, 2013, **298–299**, 37–40.
133. E. L. Cates, A. P. Wilkinson and J. H. Kim, *J. Phys. Chem. C*, 2012, **116**, 12772–12778.
134. Q. Du, G. Zhou, J. Zhou, X. Jia and H. Zhou, *J. Alloys and Comp.*, 2013, **552**, 152–156.
135. D. Ding, Y. Wu, G. Ren, J. Yang and G. Zhang, *J. Alloys and Comp.*, 2013, **546**, 296–299.
136. X. Lu and K. Zhao, *Optical Mater.*, 2012, **34**, 1926–1929.
137. X. Shen, L. Li, F. He, X. Meng and F. Song, *Mat. Chem and Phys.*, 2012, **132**, 471–475.
138. N. S. Gajbhiye, R. S. Ningthoujam, A. Ahmed, D. K. Panda, S. S. Umare and S. J. Sharma, *Pramana*, 2008, **70**, 313-321.

139. Z. Wang, P. Li, X. Zhang, Q. Li, T. Li, Z. Yang and Q. Guo, *Physica B*, 2013, **414**, 56–59.
140. L. Ya-Jun, W. Hong-Zhi, L. Yao-Gang, Z. Qing-Hong, *J. Inorg. Mater.*, 2012, **27**, 1095-1098.
141. D. M. Shi, Y. G. Zhao, X. F. Wang, G. H. Liao, C. Zhao, M. Y. Peng and Q. Y. Zhang, *Physica B*, 2011, **406**, 628–632.
142. L. Liu, Y. Wang, Y. Bai, X. Zhang, K. Yang, L. Yang and Y. Song, *J. Appl. Phys.*, 2010, **107**, 093103 -093107.
143. D. W. Cooke, B. L. Bennett, and K. J. McClellan, *Phys. Rev. B*, 2000, **61**, 11973–11978.
144. M. Haase and H. Schäfer, *Ang. Chem. Inter. Edit.*, 2011, **50**, 5808-5829.
145. G. Wakefield, E. Holland, P. J. Dobson and J. L. Hutchison, *Advanced Materials*, 2001, **13**, 1557-1560.
146. R. Schmechel, M. Kennedy, H. Seggern, H. Winkler, M. Kolbe, R. A. Fischer, Li Xiaomao, A. Benker, M. Winterer and H. Hahn, *J. Appl. Phys.*, 2001, **89**, 1679-1686.
147. F. Vetrone, J. C. Boyer, J. A. Capobianco, A. Speghini, and M. Bettinelli, *Chem. Mater.*, 2003, **15**, 2737–2743.
148. S. K. Singh, K. Kumar and S. B. Rai, *Mat Sci Engg B*, 2010, **166**, 180-184.
149. H. Guo, N. Dong, Min Yin, W. Zhang, Liren Lou and S. Xia *J. Phys. Chem. B*, 2004, **108**, 19205–19209.
150. S. K. Singh, K. Kumar and S. B. Rai, *Appl phys B*, 2010, **100**, 443-446.
151. M. Yu, J. Lin, Z. Wang, J. Fu, S. Wang, H. J. Zhang and Y. C. Han, *Chem. Mater.*, 2002, **14**, 2224–2231.
152. F. Lei and B. Yan, *J. Solid State Chem.*, 2008, **181**, 855–862.
153. Y. Su, L. Li and G. Li, *Chem. Mater.*, 2008, **20**, 6060–6067.
154. Q. Dai, H. Song, X. Bai, G. Pan, S. Lu, T. Wang, X. Ren and H. Zhao, *J. Phys. Chem. C*, 2007, **111**, 7586–7592
155. D. Jia, R. S. Meltzer, W. M. Yen, W. Jia and X. Wang, *Appl. Phys. Lett.*, 2002, **80**, 1535-1537.
156. T. Katsumata, T. Nabae, K. Sasajima, T. Matsuzawa, *J. Cryst. Growth*, 1998, **183**, 361-365.
157. T. Matsuzawa, Y. Aoki, N. Takeuchi and Y. Murayama, *J. Electrochem. Soc.*, 1996, **143**, 2670-2673.
158. N. K. Giri, S. K. Singh and S. B. Rai, *Appl. Phys. B*, 2010, **99**, 271-277

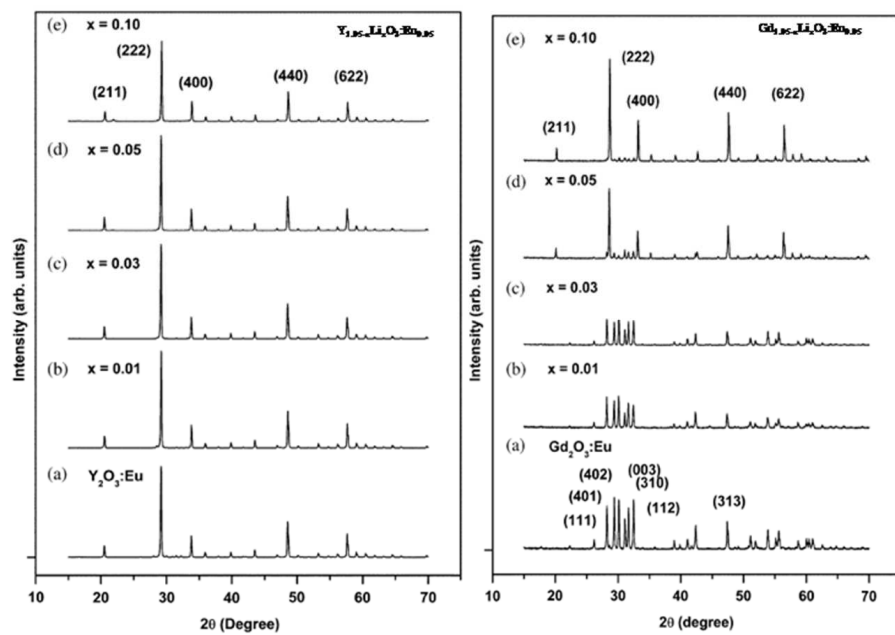
159. F. Clabau, X. Rocquefelte, S. Jobic, P. Deniard, M. H. Whangbo, A. Garcia, and T. L. Mercier, *Chem. Mater.*, 2005, **17**, 3904–3912.
160. A. Nag and T. R. N. Kutty, *J. Alloys and Comp.*, 2003, **354**, 221–231.
161. M. A. Peña and J. L. G. Fierro, *Chem. Rev.*, 2001, **101**, 1981–2018.
162. A. A. Bokov and Z. G. Ye, *J. Mater. Sci.*, 2006, **41**, 31–52.
163. H. Yamamoto, S. Okamoto and H. Kobayashi, *J. Lumins.*, 2002, **100**, 325–332.
164. V. Singh, V. K. Rai and M. Haase, *J. Appl. Phys.*, 2012, **112**, 063105–063109.
165. M. De, P. S. Ghosh and V. M. Rotello, *Adv. Mater.*, 2008, **20**, 4225–4241.
166. P. V. Kamat, *J. Phys. Chem. B*, 2002, **106**, 7729–7744.
167. Y. Gao and Z. Tang, *Small*, 2011, **7**, 2133–2146.
168. T. Schmidt, G. Müller and L. Spanhel, *Chem. Mater.*, 1998, **10**, 65–71.
169. Y. Wang, H. Cheng, Y. Hao, J. Ma, W. Li and S. Cai, *Thin Solid Films*, 1999, **349**, 120–125.
170. W. Luo, R. Li and X. Chen, *J. Phys. Chem. C*, 2009, **113**, 8772–8777.



Formatted: Font color: Black

Formatted: Font color: Black

Figure 1: (a) CIE coordinates of $\text{Ca}_{0.98}\text{SiN}_{2-2\delta/3}\text{O}_6:0.01\text{Ce}^{3+}/0.01\text{Li}^+$ and the photos of the powder sample under daylight and 365 nm UV excitation. (b) PL emission spectra of $\text{Na}_{1-y}\text{Li}_y\text{Ca}_{0.99}\text{PO}_4:\text{Eu}_{0.01}$ phosphors sintered in argon initially and later in N_2H_2 atmosphere with varying lithium ion concentrations. (c) PL spectra of $\text{CaO}:\text{Ce}^{3+}$ and $\text{CaO}:\text{Ce}^{3+}, \text{Li}^+$. The inset presents a histogram for the integrated PL intensity, where the intensity of $\text{CaO}:\text{Ce}^{3+}$ is normalized. Photographs of: (d) an as-prepared CdSe QD- and $\text{Sr}_3\text{SiO}_5:\text{Ce}^{3+}, \text{Li}^+$ phosphor-based white LED, (e) the same white light-emitting LED operated at 5 mA. (a) Reproduced from Ref. ¹⁷ with permission from The Royal Society of Chemistry. (b) Reprinted (adapted) with permission from Ref. ¹² Copyright © 2012 Elsevier B.V. All rights reserved. (c) Reprinted (adapted) with permission from Ref. ¹⁰ Copyright © 2013 Elsevier B.V. All rights reserved. (d-e) Reprinted (adapted) with permission from Ref. ⁸ Copyright © 2008 WILEY-VCH Verlag GmbH & Co. KGaA, Weinheim.



Formatted: Font color: Black

Formatted: Font color: Black

Figure 2: X-ray diffraction (XRD) patterns of $Y_{1.95-x}Li_xO_3:Eu_{0.05}$ and $Gd_{1.95-x}Li_xO_3:Eu_{0.05}$ phosphor. Reprinted (adapted) with permission from Ref.⁵⁷ Copyright © 2005 Elsevier B.V. All rights reserved.

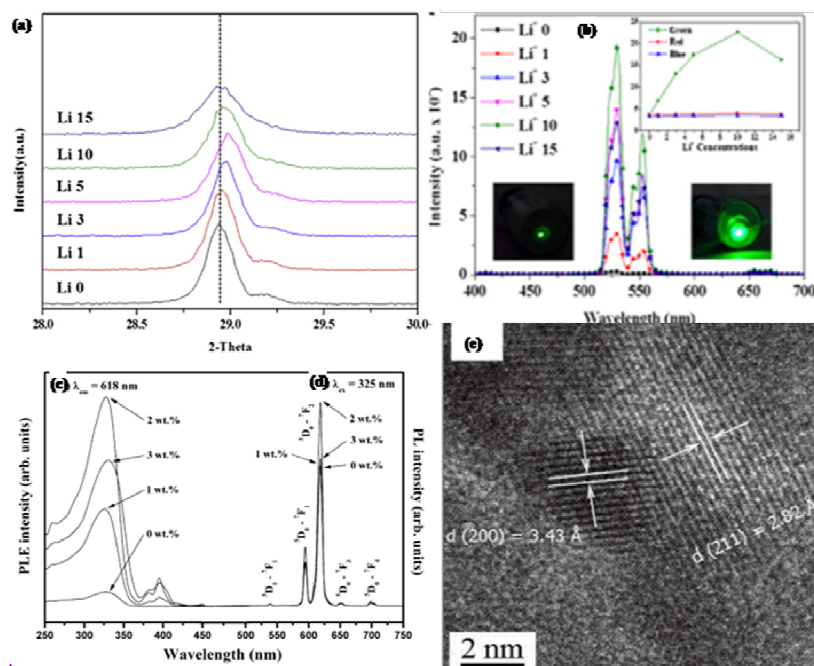


Figure 4: (a) X-ray diffraction patterns of Li⁺/Er³⁺/Yb³⁺ tri-doped CaMoO₄ upconversion phosphors (2 mol% of Er³⁺ and 8 mol% of Yb³⁺ and 0-15 mol% Li⁺) near 2θ = 29° for (112) peak. (b) Photoluminescence spectra of CaMoO₄ phosphors fixed 2 mol% of Er³⁺ and 8 mol% of Yb³⁺ with various Li⁺ concentrations from 0 to 15 mol% ranged. (c) A comparison of the room temperature (c) photoluminescence excitation (PLE) and (d) PL spectra of YVO₄:Eu³⁺ ceramics with different Li⁺ ion content. (e) High resolution transmission electron microscopy image of 500 °C annealed sample of 5 at. % Li⁺ co-doped YPO₄:5Eu. (a) and (b) Reprinted (adapted) with permission from Ref. Ref.⁷⁶ Copyright © 2012 Elsevier B. V. All rights reserved. (c) and (d) was published in Ref.⁸⁶ and reprinted with permission. Copyright © 2010 Elsevier Masson SAS. All rights reserved. (e) is taken from Ref.⁸⁴; used in accordance with the creative Commons Attribution 3.0 Unported License.

Formatted: Font color: Black

Formatted: Font color: Black

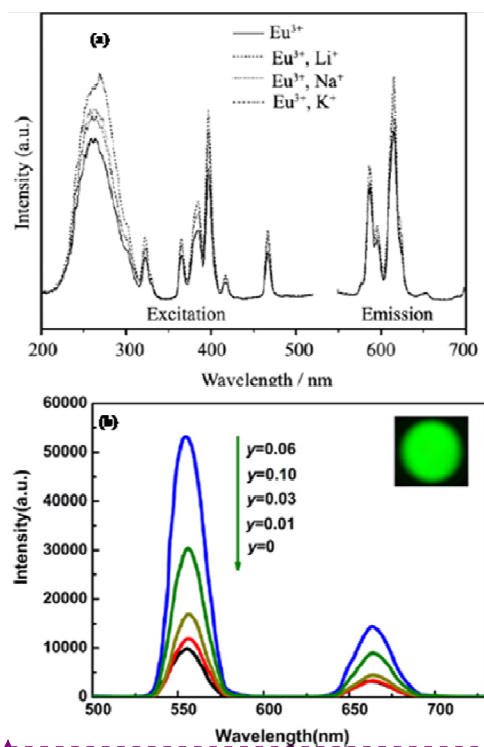


Figure 5: (a) Excitation and emission spectra of CaAl₂O₄:Eu³⁺, R⁺ (R = Li, Na, K) under 254 nm excitation and monitored at 615 nm. (b) Upconversion emission spectra of SrAl₂O₄: 0.01Ho³⁺, 0.20Yb³⁺, yLi⁺. Inset shows the picture of the emission of SrAl₂O₄: 0.01Ho³⁺, 0.20Yb³⁺, 0.06 Li⁺ ceramics under excitation wavelength 980 nm. (a) Reprinted (adapted) with permission from Ref.⁸⁹ Copyright © 2010 Elsevier. All rights reserved. (b) Reprinted (adapted) with permission from Ref.⁹⁰ Copyright © 2012 Elsevier B. V. All rights reserved.

Formatted: Font color: Black

Formatted: Font color: Black

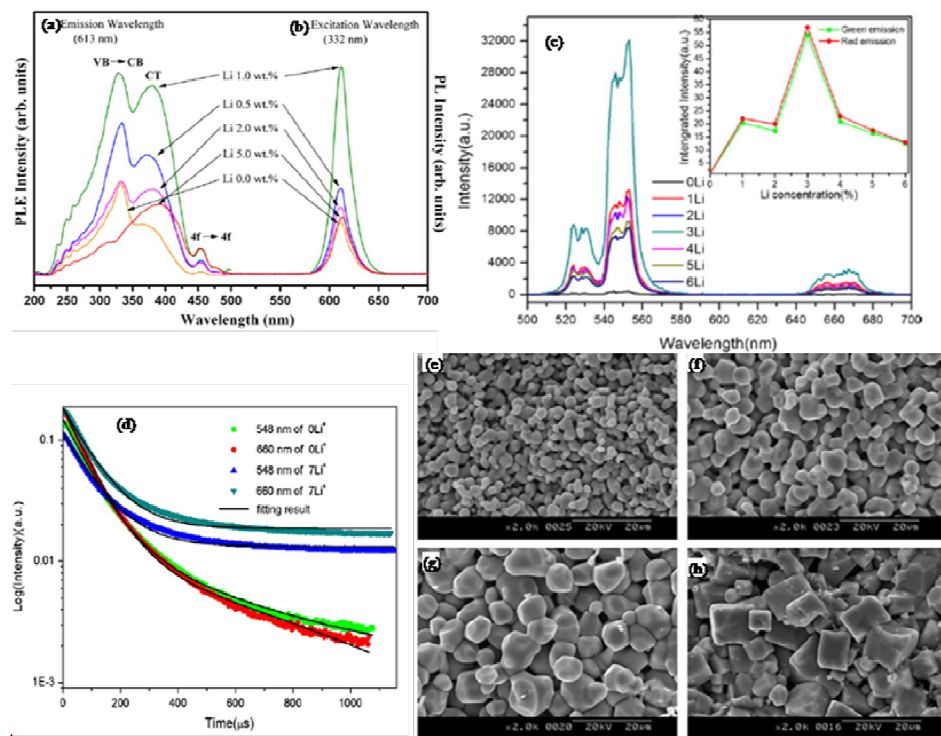


Figure 6: (a) Excitation and (b) emission spectra of $\text{CaTiO}_3:\text{Pr}^{3+}$ with different concentrations (0.5, 1, 2, and 5 wt. %) of Li^+ ions co-doped $\text{CaTiO}_3:\text{Pr}^{3+}$ phosphors. (c) Upconversion emission spectra of $\text{BaTiO}_3: 2\text{Er}^{3+}$ co-doped with 1–6 mol% Li^+ ions, under 976 nm laser excitation. Inset shows integral intensity of green and red emission as a function of the concentration of Li^+ . (d) Decay profiles of the $^4\text{S}_{3/2} \rightarrow ^4\text{I}_{15/2}$ and $^4\text{F}_{9/2} \rightarrow ^4\text{I}_{15/2}$ transitions of Er^{3+} ions in $\text{BaTiO}_3: 1\% \text{Er}^{3+}, 5\% \text{Yb}^{3+}$ and $\text{BaTiO}_3: 1\% \text{Er}^{3+}, 5\% \text{Yb}^{3+}, 7\% \text{Li}^+$ under 976 nm diode laser excitation. SEM image of (e) $\text{CaTiO}_3:\text{Pr}^{3+}$ (f) 0.5 wt.%, (g) 1 wt.%, and (h) 2 wt.%, Li-doped $\text{CaTiO}_3:\text{Pr}^{3+}$ phosphors. (a, b) and (e-h) is published in Ref.⁹⁴ and reprinted with permission. Copyright © 2011 Elsevier Masson SAS. All rights reserved. (c) Reprinted (adapted) with permission from Ref.⁹² Copyright © 2011 Elsevier B. V. All rights reserved. (d) Reprinted with permission from Ref.⁹³ Copyright © 2010 Elsevier B. V. All rights reserved.

Formatted: Font color: Black

Formatted: Font color: Black

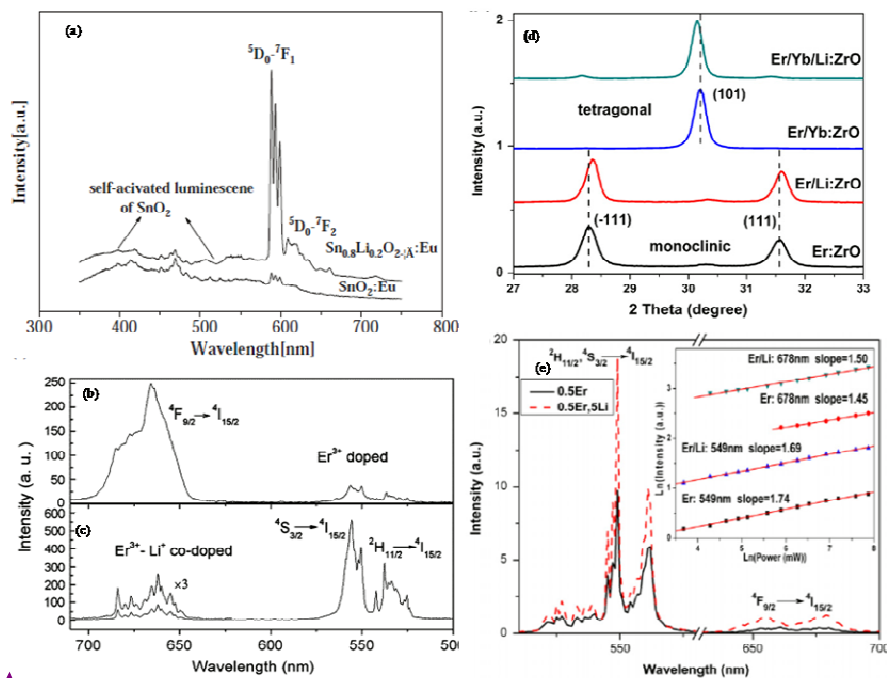


Figure 7: (a) Emission spectra of SnO₂:Eu and Sn_{0.8}Li_{0.2}O_{2.δ}:Eu under the excitation wavelength of 300 nm. Room temperature upconversion spectra of (b) Er³⁺ doped and (c) Er³⁺-Li⁺ (1.0 mol %) co-doped ZnO nanoparticles under 980 nm diode laser excitation. (d) Powder X-ray diffraction pattern of Er³⁺: ZrO₂ with and without Li⁺ ions and Er³⁺/Yb³⁺:ZrO₂ with and without Li⁺ ions in the range of 27–33°. (e) UC emission spectra of ZrO₂: Er³⁺/Li⁺ (0 or 5 mol%) nanocrystals under 976 nm excitation. Inset shows the ln-ln plot of intensity versus excitation power dependence of the green and red emissions. (a) Reprinted with permission from Ref.⁹⁹ Copyright © 2005 Elsevier B. V. All rights reserved. (b) and (c) Reprinted with permission from Ref.¹⁰² Copyright © 2008 Elsevier B. V. All rights reserved. (d) and (e) Reprinted with permission from Ref.¹⁰⁵ Copyright © 2011 Elsevier B. V. All rights reserved.

Formatted: Font color: Black

Formatted: Font color: Black

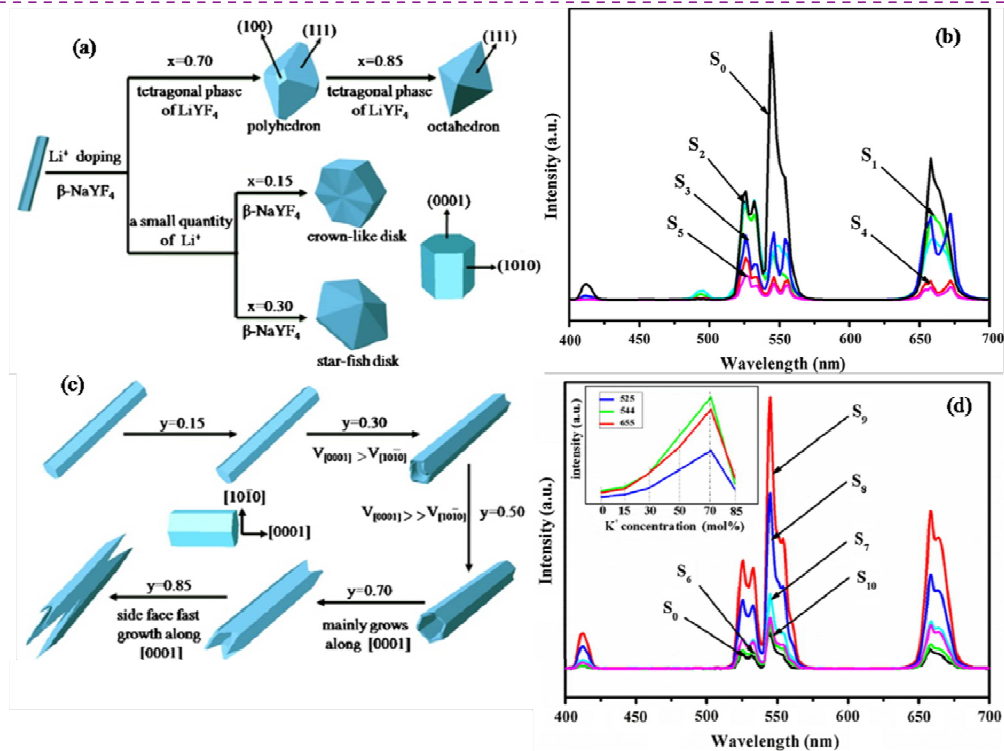
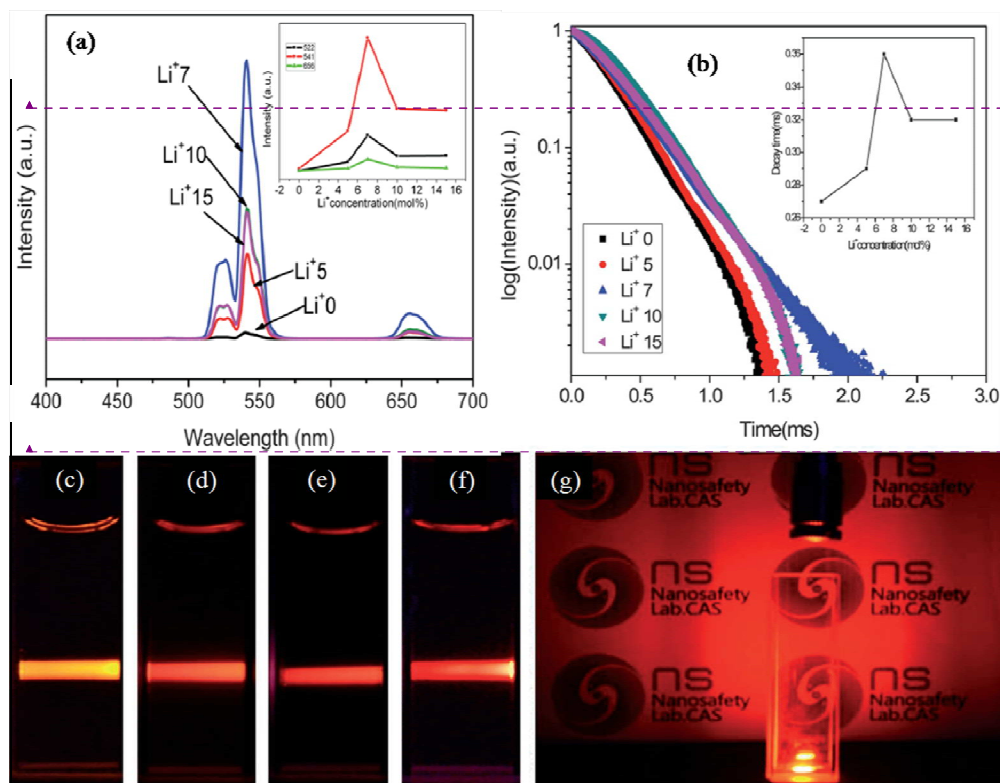


Figure 8: (a) Schematic illustration of the formation process of Li_xNa_{1-x}YF₄ with various morphologies. (b) UC luminescence spectra of the as-prepared Li_xNa_{1-x}YF₄:Yb³⁺/Er³⁺ products under 980 nm excitation at room temperature ($x = 0, 0.15, 0.30, 0.50, 0.70, 0.85$ are denoted by S₀ to S₅). (c) Schematic illustration for the possible formation process of K_yNa_{1-y}YF₄:Yb³⁺/Er³⁺ with various morphologies. (d) UC luminescence spectra of the as-prepared K_yNa_{1-y}YF₄:Yb³⁺/Er³⁺ products under 980 nm excitation at room temperature ($y = 0.15, 0.30, 0.50, 0.70, 0.85$ are denoted by S₆ to S₁₀). The inset shows the integral intensity of green and red emission as a function of the concentration of K⁺ ions. Reprinted with permission from Ref.¹⁰⁷ Copyright © 2013 Elsevier B. V. All rights reserved.

y.

Formatted: Font color: Black

Formatted: Font color: Black



Formatted: Font color: Black

Formatted: Font color: Black

Formatted: Font color: Black

Figure 9: (a) UC luminescence spectra of $\text{NaGdF}_4 : \text{Yb/Er/Li}^+$ (0–15 mol %) nanoparticles under 980 nm excitation at room temperature. The inset shows the integral intensity of green and red emission as a function of the concentration of Li^+ ions. (b) Decay profiles of ${}^4\text{I}_{11/2}/{}^4\text{I}_{13/2}$ transition in $\text{NaGdF}_4 : \text{Yb}^{3+}/\text{Er}^{3+}$ NPs with 0–15 mol% Li^+ under 980 nm excitation. (c) to (f) Luminescence photographs of calcined $\text{GdF}_3:\text{Yb,Er}$ (20, 2 mol%) UCNPs (having 0, 5, 10 and 25 mol% of Li^+) dispersed in deionized water. (g) Solid powder (0.20 g) of $\text{GdF}_3:\text{Yb,Er,Li}$ (25 mol%) UCNPs was placed into a quartz vessel and excited under a 980 nm laser to visually demonstrate the naked-eye-visible brilliant red light. (a-b) Reproduced from Ref.¹¹¹ with permission from The Royal Society of Chemistry. (c-g) Reprinted with permission from Ref.¹⁰⁸ Copyright © 2012 Wiley-VCH Verlag GmbH&Co. KGaA, Weinheim.

Table 1: Principal luminescent transitions in lanthanide ions (Ln³⁺)

Ln	Transition	Emission wavelength (nm)	Remark
Pr	$^3P_2 \rightarrow ^3H_4$	440	Weak, QC
	$^3P_0 \rightarrow ^3H_4$	480	Strong, UC and QC
	$^1D_2 \rightarrow ^3F_4$	1037 (P, NIR)	Medium, UC and QC
Nd	$^2P_{3/2} \rightarrow ^4I_{11/2}$	410	Strong, UC and QC
	$^2P_{3/2} \rightarrow ^4I_{13/2}$	452	Strong, UC and QC
	$^4F_{3/2} \rightarrow ^4I_{11/2}$	1064 (F, NIR)	Strong, QC and DS
Sm	$^4G_{5/2} \rightarrow ^6H_{7/2}$	601 (P, Orange)	Strong, DS
Eu	$^5D_0 \rightarrow ^7F_{0,1,2,3,4}$	570-720 (P, Orange)	Strong, UC and DS
Tb	$^5D_4 \rightarrow ^7F_{6,5,4,3}$	480-650 (P, Green)	Strong, UC, DS and QC
Dy	$^4F_{9/2} \rightarrow ^6H_{15/2}$	486	Medium, DS and QC
	$^4F_{9/2} \rightarrow ^6H_{13/2}$	575(P, Yellow-Orange)	Strong, DS and QC
Ho	$^5S_2, ^5F_4 \rightarrow ^5I_8$	540 (F, Green)	Strong, UC and QC
	$^5F_5 \rightarrow ^5I_8$	644(F, Red)	Strong, UC and QC
	$^5I_6 \rightarrow ^5I_8$	1180(NIR)	Strong, QC
Er	$^4S_{3/2} \rightarrow ^4I_{15/2}$	545 (F, Green)	Strong, UC and QC
	$^4F_{9/2} \rightarrow ^4I_{15/2}$	665 (F, Red)	Strong, UC and QC
	$^4I_{13/2} \rightarrow ^4I_{15/2}$	1540 (NIR)	Strong, QC
Tm	$^1D_2 \rightarrow ^3F_4$	450 (Blue)	Medium, UC and QC
	$^3H_4 \rightarrow ^3H_6$	800 (NIR)	Strong, UC and QC
Yb	$^2F_{5/2} \rightarrow ^2F_{7/2}$	980 (F, NIR)	Strong, UC, QC and DS

□QC-quantum-cutting, DS-down-shift, UC-upconversion, NIR-near-infrared, P-Phosphoresce, F-Fluorescence. Most of the data presented are taken from Ref.^{31,52}

Table 2: Effect of Li⁺ ion on the luminescence properties of Ce³⁺ and Eu²⁺ ions doped in different host matrices

Sample	Change in luminescence properties	Remark
CaBr:Eu ²⁺ , Li ⁺ ⁷	improves radiation hardness	by reducing the X-ray induced vacancy centers
Li ₂ CaSiO ₄ :Eu ²⁺ ⁸	small Stokes Shift	smaller ionic radius of Li ⁺ constrain the distortion of the excited state
CaS:Ce ³⁺ , Pr ³⁺ , Li ⁺ ⁹	3 times enhanced afterglow intensity and 4 times enhancement in afterglow time	new cation vacancy formed which work as electron trap center
CaO: Ce ³⁺ , Li ⁺ ¹⁰	1.88 times enhancement in luminescence intensity	increased absorbance to the excitation photons
SrAl ₂ O ₄ :Eu ²⁺ , Ce ³⁺ , Li ⁺ ¹¹	enhanced luminescence of Eu ²⁺	charge compensation
NaCaPO ₄ :Eu ²⁺ , Li ⁺ ¹²	enhanced luminescence of Eu ²⁺	change in spin-orbit coupling and coordination of Eu ²⁺ ions
Sr _{2-2x} LiSiO ₄ F:xCe ³⁺ , xLi ⁺ ¹³	shift in peak position	Ce ³⁺ occupying different Sr ²⁺ site
Sr ₃ SiO ₅ : Ba ²⁺ , Ce ³⁺ , Li ⁺ ¹⁴	Li ⁺ co-doping helps to incorporate Ce ³⁺ ions on Sr ²⁺ site	by charge compensation
Lu ₂ SiO ₅ : Ce ³⁺ , Li ⁺ ¹⁵	2.2 times enhancement in luminescence intensity	change in crystal field around Ce ³⁺ ions
Sr ₃ Si ₂ O ₄ N ₂ : Eu ²⁺ , Li ⁺ ¹⁹	red shift in emission band	re-absorption in Eu ²⁺ ions
Sr ₃ Si ₂ O ₄ N ₂ : Ce ³⁺ , Li ⁺ ¹⁹	no prominent red shift	

Table 3: Luminescence enhancement (and their explanation) in various activators during down-shifting and upconversion processes in Y_2O_3 and Gd_2O_3 in the presence of Li^+ ion

Sample	DS/UC	Luminescence Enhancement	Remark
$Gd_{1.84}Li_{0.08}Eu_{0.08}O_3$ ⁵⁶	DS	2.3 times (PL)	improved crystallinity, higher surface roughness and increased optical phonon energy
$Y_{1.9}Li_{0.05}Eu_{0.05}O_3$ ⁵⁷	DS	2.5 times (CL)	charge compensation
$Gd_{1.92}Li_{0.03}Eu_{0.05}O_3$ ⁵⁷	DS	3 times (PL)	lowering of local symmetry
$Gd_{1.9}Li_{0.06}Eu_{0.04}O_3$ ⁵⁸	DS	4 times (PL)	charge compensation and lowering of local symmetry
$Gd_{1.84}Li_{0.08}Eu_{0.08}O_3$ ⁵⁹	DS	2.3 times (PL)	improved crystallinity and higher surface roughness
$Gd_{1.87}Li_{0.06}Yb_{0.06}Tm_{0.01}O_3$ ⁶⁰	UC	10 times (PL)	lowering of symmetry around Tm^{3+} and decrease in OH concentration
$Gd_{1.935}Li_{0.04}Yb_{0.02}Ho_{0.005}O_3$ ⁶¹	UC	10 times (PL)	lowering of symmetry around Ho^{3+}
$Y_{1.935}Li_{0.05}Nd_{0.015}O_3$ ⁶²	UC	2 times (PL)	changed morphology, modification of local symmetry and decrease in OH concentration
$Y_{1.92}Li_{0.05}Yb_{0.02}Er_{0.01}O_3$ ⁶³	UC	30 times (PL)	prolong lifetime of their intermediate states
$Y_{1.92}Li_{0.05}Yb_{0.02}Er_{0.01}O_3$ ⁶⁴	UC	25 times (PL)	change in crystal field, prolong lifetime of intermediate states, increased optical active sites and dissociation of clusters
$Y_{1.94}Li_{0.04}Er_{0.02}O_3$ ⁶⁵	UC	10 times (PL)	change in crystal field and dissociation of clustering.
$Y_{1.94}Li_{0.05}Er_{0.01}O_3$ ⁶⁶	UC	45 times (PL)	tailored lifetime of intermediate levels, suppressed cross relaxation and enlarged particle size
$Y_{1.94}Li_{0.05}Er_{0.01}O_3$ ⁶⁷	UC	45 times (PL)	tailored lifetime of intermediate levels
$Y_{1.84}Li_{0.08}Eu_{0.08}O_3$ ⁶⁸	DS	1.2 times (EL)	improved crystallinity and higher surface roughness
$Y_{1.70}Li_{0.1}Eu_{0.2}O_3$ ⁶⁹	DS	1.2 times (PL)	Improved morphology
$Y_{1.9455}Li_{0.05}Yb_{0.05}Tm_{0.0025}O_3$ ⁷¹	UC	15 times (PL)	change in crystal field, decrease in OH concentration and dissociation of clusters
$Y_{1.9}Li_{0.05}Yb_{0.05}O_3$ ⁷²	DS	12 times (PL)	change in crystal field
$Y_{1.93}Li_{0.05}Tm_{0.02}O_3$ ⁷³	UC	19 times (PL)	increase in lifetime of intermediate levels
$Y_{1.917}Li_{0.05}Yb_{0.03}Er_{0.003}O_3$ ⁷⁴	UC	3 times (PL)	change in crystal field and decrease in OH concentration

Table 4: Luminescence enhancement (and their explanation) in various activators during down-shifting and upconversion processes in ABO₄ type of host in presence of Li⁺ ions

Sample	DS/UC	Luminescence Enhancement	Remark
Ca _{0.8} Li _{0.1} Er _{0.02} Yb _{0.08} MoO ₄ ⁷⁶	UC	83 times (PL)	local crystal field distortion around Er ³⁺ ion
Ca _{0.95} MoO ₄ :0.05Dy ³⁺ ,0.05Li ⁺ ⁷⁷	DS	1.3 times (PL)	charge compensation
Ca _{0.95} MoO ₄ :0.05Tb ³⁺ ,0.05Li ⁺ ⁷⁸	DS	- (PL)	oxygen vacancy
Li _{0.05} Eu _{0.05} La _{0.9} PO ₄ ⁷⁹	DS	2 times (PL)	decrease in interstitial oxygen and reduced internal reflections
La _{0.93} Eu _{0.07} VO ₄ : 0.25 wt.% Li ⁸⁰	DS	- (PL)	oxygen vacancy, increased grain size
YPO ₄ :2 at. % Dy, 7 at. %Li ⁸¹	DS	- (PL)	improved crystallinity
YPO ₄ : 5% Eu ³⁺ , 5% Li ⁺ ⁸²	DS	2.5 times (PL)	increased crystallinity and grain size
YPO ₄ : 5% Eu ³⁺ ,3% Li ⁺ ⁸³⁻⁸⁵	DS	- (PL)	increased crystallinity
YVO ₄ : 0.03% Eu ³⁺ ,2% Li ⁺ ⁸⁶	DS	1.43 (PL)	increased crystallinity and surface roughness
YVO ₄ : 0.03% Eu ³⁺ ,1% Li ⁺ ⁸⁷	DS	1.7 (PL)	increased crystallinity and surface roughness

Table 5: Luminescence enhancement (and their explanation) in various activators during down-shifting and upconversion processes in perovskite host in presence of Li^+ ions

Sample	DS/UC	Luminescence Enhancement	Remark
BaTiO_3 : 2% Er^{3+} , 3% Li^+ ⁹²	UC	56 times	local crystal field distortion around Er^{3+} , reduction in OH concentrations
BaTiO_3 : 1% Er^{3+} , 5% Yb^{3+} , 7% Li^+ ⁹³	UC	10 times	local crystal field distortion around Er^{3+} ions
CaTiO_3 : Pr^{3+} , 1% Li^+ ^{94, 95}	UC	3.5 times	improved crystallinity, increase in surface roughness
CaZrO_3 : 5% Eu^{3+} , 10% Li^+ ⁹⁶	DS	3 times	charge compensation
SrZnO_3 : Eu^{3+} , M^+ (Li, Na, K) ⁹⁷	DS	-	charge compensation

Table 6: Luminescence enhancement (and their explanation) in different activators during down-shifting and upconversion processes in metal oxide nanoparticles host in presence of Li^+ ions

Sample	DS/UC	Luminescence Enhancement	Remark
MgO: 1.5% Dy^{3+} , 20% Li^{+98}	DS	4 times (PL)	improved crystallinity, increased grain size, change size, change in crystal field around Dy^{3+} ions
SnO_2 : Eu^{3+} , Li^{+99}	DS	14 times (PL)	improved crystallinity, increased grain size, increased oxygen vacancy
TiO_2 : Er^{3+} , Yb^{3+} , Li^{+101}	UC	215 times (PL)	change in local crystal field around Er^{3+} ion
ZnO : Er^{3+} , Li^{+102}	UC	PL switching (red to green)	change in local crystal field around Er^{3+} ion increased crystallinity
ZnO : Dy^{3+} , Li^{+103}	DS	10 times (PL)	radiative recombination of the large amount of trapped carriers excited from ZnO host, improved crystallinity
ZnO : Er^{3+} , Li^{+104}	UC	120 times (PL)	change in local crystal field around ions reduced OH group concentration
ZrO_2 : Er^{3+} , Yb^{3+} , Li^{+105}	UC	1.5 times (PL)	change in local crystal field around ions increased grain size

Table 7: Effect of Li⁺ ion on the UC luminescence of lanthanide ions doped in fluoride host matrices

Sample	Change in luminescence properties	Remark
NaYF ₄ :Yb ³⁺ /Er ³⁺ ,K ⁺ /Li ⁺ ¹⁰⁷	UC emission intensity decreases on Li ⁺ doping, whereas it increases on K ⁺ doping	change in morphology and crystal structure on Li ⁺ doping and lowering of crystal symmetry around Er ³⁺ ions in K ⁺ doping
GdF ₃ :Yb ³⁺ /Er ³⁺ , Li ⁺ ¹⁰⁸	change in UC emission color from yellow to red, red emission is 8 times higher than in NaGdF ₄ :Yb ³⁺ /Er ³⁺	change in crystal symmetry around Er ³⁺ ions, back energy transfer
NaYbF ₄ :Yb ³⁺ /Er ³⁺ , Li ⁺ ¹⁰⁹	UC color tunability	change in crystal symmetry around Er ³⁺ ions and weakened polarization effect
NaYF ₄ :Yb ³⁺ /Tm ³⁺ ,K ⁺ /Li ⁺ ¹¹⁰	decrease in concentration quenching	crystal distortion and increased crystal size
NaGdF ₄ :Yb ³⁺ /Er ³⁺ , Li ⁺ ¹¹¹	enhanced UC luminescence	change in crystal symmetry around Er ³⁺ (47 times for green and 23 for red), increased crystal size, increased paramagnetism lifetime of ⁴ S _{3/2} state, decrease in distance between Gd ³⁺ ions (for increased paramagnetism)
ErF ₃ :Er ³⁺ , Li ⁺ ¹¹²	four times enhancement in UC emission	change in crystal symmetry around Er ³⁺ ions
Lu ₆ O ₅ F ₈ :Yb ³⁺ /Er ³⁺ , Li ⁺ ¹¹³	increased UC emission	change in crystal symmetry around Er ³⁺ ions, increased crystallinity, reduced quenching centers (OH ⁻)
NaYF ₄ :Yb ³⁺ /Er ³⁺ ,K ⁺ /Li ⁺ ¹¹⁴	color tunability of UC emission	change in crystal structure and lowering of crystal symmetry around Er ³⁺ ions

Table 8: Luminescence enhancement (and their explanation) in different activators during down-shifting and upconversion processes in miscellaneous host in presence of Li⁺ ions

Sample	DS/UC	Luminescence Enhancement	Remark
Ba ₂ GdNbO ₆ : Eu ³⁺ /Dy ³⁺ , Li ⁺ 115	DS	-	improved crystallinity, increased grain size
BaZn ₂ (PO ₄) ₂ : Sm ³⁺ , R ⁺ 116	DS	-	charge compensation
R ⁺ ((Li, Na, K))			
Ca ₃ B ₂ O ₆ : Dy ³⁺ , Li ⁺ 117	DS	-	charge compensation, flux effect, change in local environment around Dy ³⁺ ions
CaSO ₄ : Tm ³⁺ /Dy ³⁺ , Li ⁺ 118	TL	-	creation of charge trap centers
(Y, Gd)BO ₃ : Tb ³⁺ , Li ⁺ 119	DS	-	spherical and non-agglomerated, particles, strong lattice distortion
YNbTiO ₆ : Eu ³⁺ , Li ⁺ 120	DS	3 times	improved crystallinity, increased grain size
YBO ₃ : Eu ³⁺ , Li ⁺ 121	DS	-	improved crystallinity, increased grain size
Zn ₂ SiO ₄ : Yb ³⁺ , Er ³⁺ , Li ⁺ /Bi ³⁺ 122	UC	-	change in local environment around Er ³⁺
SrB ₄ O ₇ : Eu ²⁺ , Li ⁺ 123	DS	-	change in electric field distribution in lattice structure
Lu ₂ SiO ₅ : Ce, Li ⁺ 125	DS	2.2 times	change in crystal field around Ce ³⁺
Y ₂ MoO ₆ : Eu ³⁺ , Li ⁺ 126	DS	-	improved crystallinity
NaSrBO ₃ : Tb ³⁺ , Li ⁺ 127	DS	-	charge compensation
Sr ₂ SiO ₄ : Eu ³⁺ , (Li ⁺ , Na ⁺ , K ⁺) 129	DS	-	charge compensation
CaSnO ₃ : Tb ³⁺ (Li ⁺ , Na ⁺ , K ⁺) 131	DS	-	charge compensation
Gd ₆ MoO ₁₂ : Li ⁺ /Ln ³⁺ 132 (Ln ³⁺ = Yb ³⁺ /Er ³⁺ /Tm ³⁺)	UC	-	change in crystal symmetry around Ln ³⁺
Y ₂ SiO ₅ : Pr ³⁺ , Li ⁺ 133	UC	9 times	change in crystal symmetry around lanthanide ions, reduction in activator ions clustering
Y ₂ Zr ₂ O ₇ : Dy ³⁺ , Li ⁺ 134 (Ln ³⁺ = Yb ³⁺ /Er ³⁺ /Tm ³⁺)	UC	2 times	improved crystallinity
Li _x Ca _{1-2x} Eu _x Si _y Mo _{1-y} O ₄ 136	DS	-	charge compensation
Ca ₂ BO ₃ Cl: Sm ³⁺ (Li ⁺ , Na ⁺ , K ⁺) 139	DS	-	charge compensation
CaSi ₂ O ₂ N ₂ : Eu ²⁺ , Dy ³⁺ , Li ⁺ 140	DS	-	charge compensation